A High-Throughput Screening Platform for Engineering Poly(ethylene Terephthalate) Hydrolases

Thomas M. Groseclose,[#] Erin A. Kober,[#] Matilda Clark, Benjamin Moore, Shounak Banerjee, Victoria Bemmer, Gregg T. Beckham, Andrew R. Pickford, Taraka T. Dale, and Hau B. Nguyen*

Cite This: *ACS Catal.* 2024, 14, 14622−14638

Read Online

ACCESS | Metrics & More | Article Recommendations | Supporting Information

ABSTRACT: The ability of enzymes to hydrolyze the ubiquitous polyester, poly(ethylene terephthalate) (PET), has enabled the potential for bioindustrial recycling of this waste plastic. To date, many of these PET hydrolases have been engineered for improved catalytic activity and stability, but current screening methods have limitations in screening large libraries, including under high-temperature conditions. Here, we developed a platform that can simultaneously interrogate PET hydrolase libraries of 10^4–10^5 variants (per round) for protein solubility, thermostability, and activity via paired, plate-based split green fluorescent protein and model substrate screens. We then applied this platform to improve the performance of a benchmark PET hydrolase, leaf-branch compost cutinase, by directed evolution. Our engineered enzyme exhibited higher catalytic activity relative to the benchmark, LCC-ICCG, on amorphous PET film coupon substrates (∼9.4% crystallinity) in pH-controlled bioreactors at both 65 °C (8.5% higher conversion at 48 h and 38% higher maximum rate, at 2.9% substrate loading) and 68 °C (11.2% higher conversion at 48 h and 43% higher maximum rate, at 16.5% substrate loading), up to 48 h, highlighting the potential of this screening platform to accelerate enzyme development for PET recycling.

KEYWORDS: *poly(ethylene terephthalate) (PET), PET hydrolase, protein engineering, high-throughput screening, directed evolution, enzymatic plastic degradation, plastic recycling, split GFP*
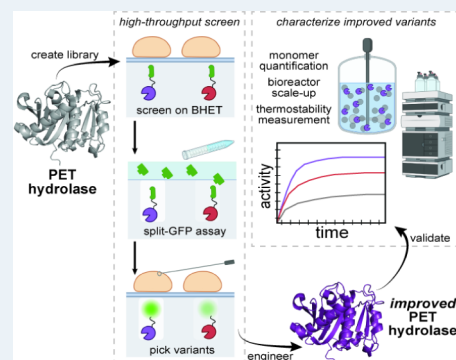
INTRODUCTION

Recent years have witnessed a massive increase in scientific work on PET hydrolases,[1−7] which are enzymes that can depolymerize poly(ethylene terephthalate) (PET) to its constituent monomers via hydrolysis of its ester bonds. Currently, PET, prevalent in packaging and textiles, is one of the most highly produced plastics globally.[8−10] Researchers have identified natural enzymes that can depolymerize PET[11−16] and have engineered and evolved them for improved function, including properties such as thermostability,[17−22] catalytic performance,[17,19−21] and substrate/product tolerance.[23,24] One of the most efficient PET hydrolases is LCC-ICCG, a quadruple mutant of leaf-branch compost cutinase (LCC), a thermotolerant PET hydrolase,[13] which was conferred with enhanced thermostability and activity through rational design of a disulfide bond and saturation mutagenesis near the active site.[17] The resulting variant, LCC-ICCG, can hydrolyze PET to terephthalic acid (TPA), ethylene glycol (EG), and mono-(2-hydroxyethyl) terephthalate (MHET),[17] which can be further broken down by MHETase to monomers[25] (Scheme 1), demonstrating the potential for these enzymes to be used in industrial PET recycling.

PET depolymerization has been reported to be most optimal at temperatures around 70 °C for thermostable PET hydrolases.[6,17,26,27] It is at this temperature, T_{opt}, that the polymer chain mobility is increased for enzymatic accessibility.[17,26,27] At higher temperatures, however, recrystallization of polymer chains has been found to reduce the rate and extent of depolymerization.[17,26,27] Recent studies have shown that the glass transition temperature (T_g) is an insufficient standard for enzymatic PET depolymerization, as T_g is typically reported for the polymer under dry conditions and decreases when being soaked in water, whereas T_{opt} considers the balance between real PET T_g in reactions and recrystallization.[26−29]

To date, PET hydrolase engineering has focused on rational and semirational design approaches,[5,6] in which single mutants and/or site-saturation mutant libraries have been constructed based on structural inspection, homology, domain swapping, and modeling. The performance screening in these cases has typically involved mass loss[15,19,30] or release of fluorogenic probes[31] from polymers, which are low-throughput and only
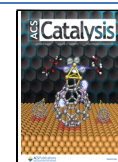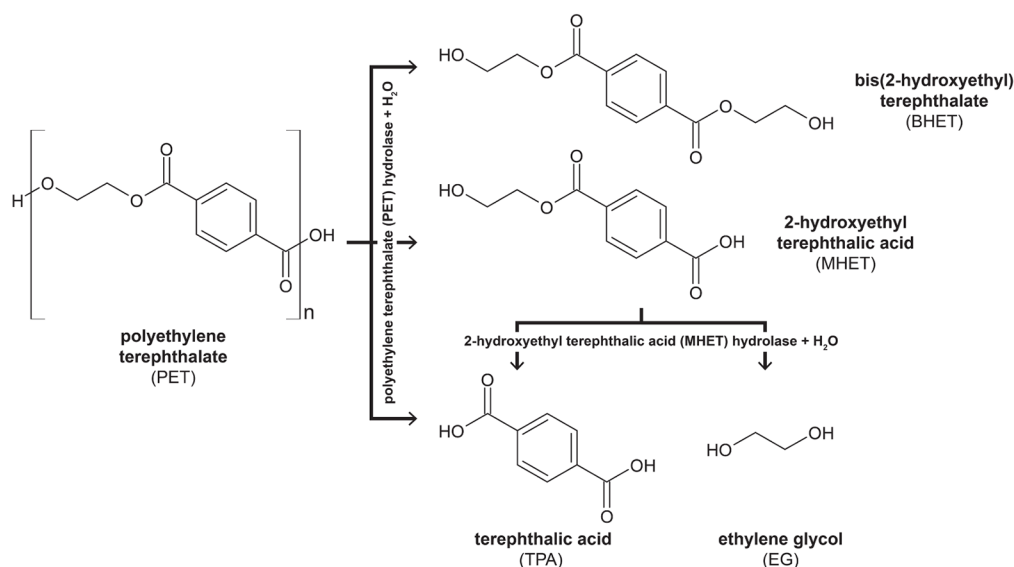
Scheme 1. PET Hydrolases Digest PET to Bis(2-hydroxyethyl) terephthalate (BHET), MHET, TPA, and EG[a]

[a]MHETases break down MHET to TPA and EG.

able to screen ~10 enzyme variants simultaneously. For larger libraries, microwell plate-based screens have been used to measure reaction products via colorimetric,[32] absorbance,[33,34] and fluorescence[35−37] readouts, or via direct product quantification using high-pressure liquid chromatography (HPLC),[16,21] but these methods are limited to screening 10^2 to 10^3 enzyme variants simultaneously. Other studies have used model substrates with multiple screening steps, culminating in a final screen on PET.[38] However, these screening assays have often been performed at low temperatures for several days, limiting the ability to discover mutations conferring increased thermostability.[38] Other assays based on halo formation have been used as an alternative method to screen for thermostable PET hydrolases.[39] In addition, PET nanoparticle suspensions have been used in several studies to detect PET depolymerization activity via turbidity changes.[19,29] While PET nanoparticles may be ideal substrates for agar plate-based screening assays, low PET hydrolysis activity, due to the small amount of enzymes released, may render screening at the colony level difficult.[19,29] Toward high-throughput (HT) evolutionary approaches, Bell et al. demonstrated improvement in the activity and thermostability of the *Ideonella sakaiensis* PETase (*Is*PETase) through targeted, semirational directed evolution.[21] This study evaluated ~2000 enzyme variants in ~2 days.[21] Recent developments of new bacterial TPA biosensor systems offer promising biosensor-based screening approaches for PET hydrolysis products, which may enable large library screening for PET hydrolases.[40−42] Additionally, a recent ultrahigh-throughput directed evolution method for PET hydrolases using a yeast display platform allowed for the evaluation of >10^7 enzyme variants.[43] While this platform screened an impressive library size, the screening was done at room temperature, therefore limiting its ability to identify beneficial mutations for improved activity near the T_{opt} of 70 °C. Ideally, an efficient PET hydrolase engineering platform would include screening large libraries ($\geq 10^4$) via selection pressure for higher PET depolymerization activity at temperatures near 70 °C.

To that end, we developed an integrated platform for engineering PET hydrolases by directed evolution with random mutagenesis. This platform couples a split green fluorescent protein (split GFP) assay,[44] which has been previously employed in protein engineering,[45,46] for quickly evaluating enzyme expression, solubility, and thermostability without the need for purification, and a model substrate assay using BHET for activity screening, followed by HT characterization on actual PET substrates. BHET was selected as a model substrate due to its similar bond type as to PET, and the hydrolysis of BHET on agar plates created visible signals (clearing zones or halos) that could easily be detected. This platform allowed us to screen enzyme libraries for both activity and expression/thermostability concurrently. In addition, this platform can simultaneously screen ~10^4 colonies or more for enhanced enzyme expression, thermostability, and depolymerization activity near the T_{opt} of 70 °C in ~2−3 days and is readily scalable. We then demonstrated the utility of this platform by improving the catalytic performance of the LCC scaffold toward amorphous PET film substrates through directed evolution. We expect that this platform will expand the ability to rapidly screen, evolve, and characterize PET hydrolase enzymes, thus contributing toward more efficient enzymatic PET depolymerization reactions for improved recycling processes.

■ RESULTS

An Integrated Platform for Engineering PET Hydrolases. Toward directed evolution via random mutagenesis, we developed a screening platform that can efficiently assess PET hydrolase libraries of $\geq 10^4$ variants simultaneously, per evolution round, for multiple properties that are deterministic of enzyme function and process viability, including protein expression and solubility, thermostability near 70 °C, and catalytic performance. An overview of our PET hydrolase engineering platform is shown in Figure 1. Briefly, our platform consists of four components: i) creating a large, random mutagenesis library via DNA shuffling (Figure 1a), ii) an HT ($\geq 10^4$ variants) colony-level coscreening assay to interrogate
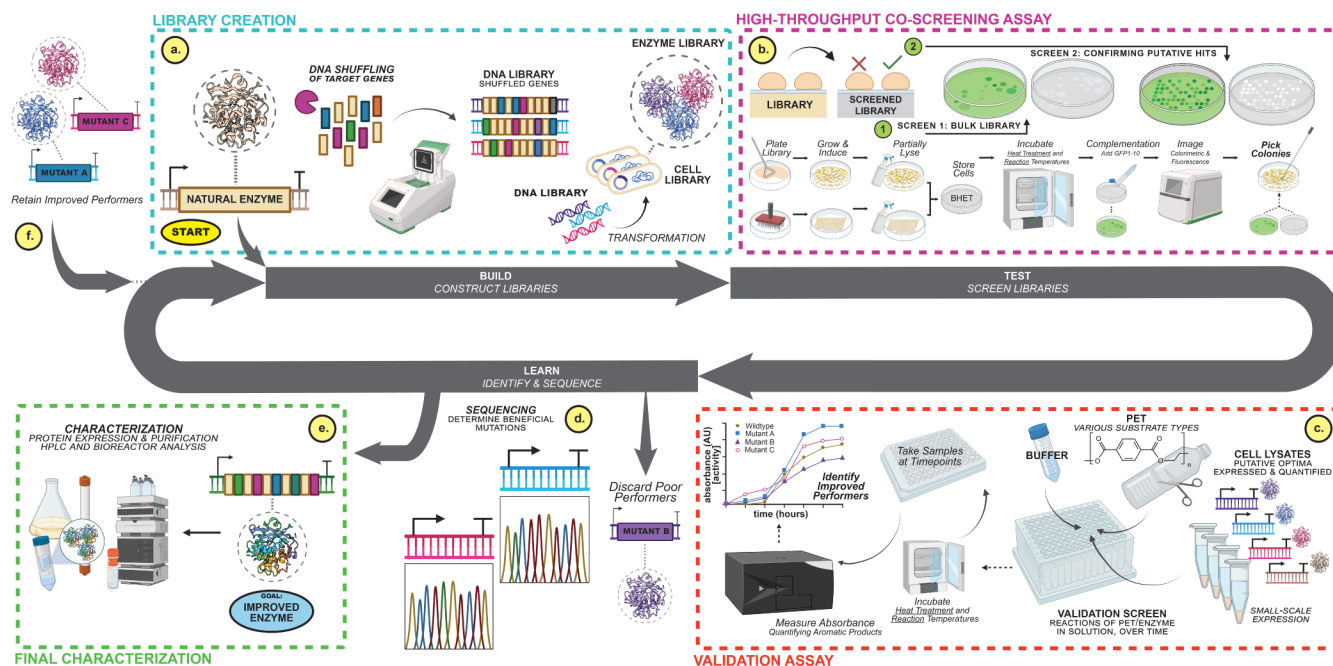
Figure 1. PET hydrolase engineering platform. a. DNA libraries were constructed from the open reading frame encoding for a starting enzyme, or selected variants from previous rounds of evolution, by DNA shuffling, cloned into the screening vector, and transformed into the expression host, *E. coli*. b. Enzymes were screened using the HT coscreening assay developed in this work. First, (1) the bulk library (>10^4 variants) was screened, then (2) putative hits (~10^2) were verified. Enzyme libraries were expressed by first growing the cell library on semipermeable membranes on plates overnight and then transferring the membranes to plates including IPTG for induction. Membranes were then moved to BHET agar screening plates, colonies were partially lysed, and membranes were returned to growth for later colony picking. This allowed the cell lysates to diffuse through the membrane onto the BHET agar plates. The BHET screening plates were then incubated at the reaction temperature, 65−70 °C, until clearing zones (halos, indicating BHET hydrolysis) appeared or if desired, the plates were preheated at 80 °C before progressing to the hydrolytic reaction. Following the reaction and complementation with GFP1−10, improved enzyme variants, chosen based on higher BHET activity (larger clearing zones) or better expression levels (higher fluorescence intensities), were traced to the original colonies grown on the membranes, allowing for colonies to be picked. c. Putative improved variants were tested on either an amorphous PET film or high-crystallinity PET powder in suspension in validation assays (~10^1 −10^2 variants). Enzyme variants were expressed on a small scale (1−5 mL), cell pellets were sonicated, and enzymes were quantified in crude cell lysates using split GFP complementation with known protein standards. Cell lysates were then normalized based on quantified enzyme concentration and added to reactions with the PET substrate. Enzymatic activity was monitored over time with PET breakdown products measured via UV absorbance. d. Identified improved enzyme variants were isolated and sequenced. After several rounds of directed evolution, if an enzyme was significantly improved (e.g., with higher activity and higher thermostability), it was chosen for final characterization including large-scale (liter scale) expression and purification, performance assessment with HPLC-based product quantitation, and measurement of PET hydrolysis in pH-controlled bioreactors. f. Otherwise, improved enzyme variants were used as parents for the next round of directed evolution, toward the goal of iteratively improving enzymes for higher performance vs selection pressures.

our large libraries simultaneously for activity, expression, and solubility of enzyme variants on BHET model substrate agar plates (Figure 1b), followed by iii) a validation (~10^2 variants) screening assay with cell lysates using either amorphous PET film or high-crystallinity PET powder substrates to identify enzyme variants with higher activity on PET substrates selected from (ii) (with improved BHET hydrolysis) (Figure 1c), and iv) characterization of final enzyme optima (1 to 10 variants) using purified enzymes with various PET substrates including amorphous PET film, amorphous PET powder, and high-crystallinity PET powder (Figure 1e). Integrated into our directed evolution platform, this enabled us to generate random mutagenesis libraries from starting enzyme scaffolds, screen them under different selection pressures (e.g., increased temperature and increased substrate concentration), select improved enzyme variants, and verify their improved properties and sequences (Figure 1d,f), with each round of evolution taking approximately 6−8 weeks. Improved enzyme variants were pooled to proceed to further rounds of directed evolution as parents, beginning the directed evolution cycle anew. After several rounds of directed evolution, we selected final enzyme

optima for detailed performance analysis using aromatic monomer product quantification by HPLC and measurement of PET hydrolysis in pH-controlled bioreactors.

A HT Coscreening Assay for Screening PET Hydrolase Libraries. The first step in this platform was the HT coscreening assay that assessed the large libraries of enzyme variants at the colony level for activity and solubility on model substrate agar plates. A detailed depiction of how the HT coscreening assay worked is shown in Figure 2. Specifically, it involves two simultaneous steps: 1) assessing enzyme solubility and concentration by split GFP complementation and 2) evaluating activity by reaction with BHET as a model substrate. Each of the enzymes in the libraries generated was genetically tagged with GFP11, a β-strand 11 of split GFP via a linker[44] (Figure 2a). Tagging enzymes with GFP11 allowed for rapid quantification of expressed and soluble enzymes by measuring the concentration in crude cell lysates, in solutions, or on agar plates via green fluorescence readout (Figure 2b), thus eliminating the need for protein purification during the screening steps. When GFP11-tagged enzymes were complemented with GFP1−10 (GFP β-strands 1−10), full-length
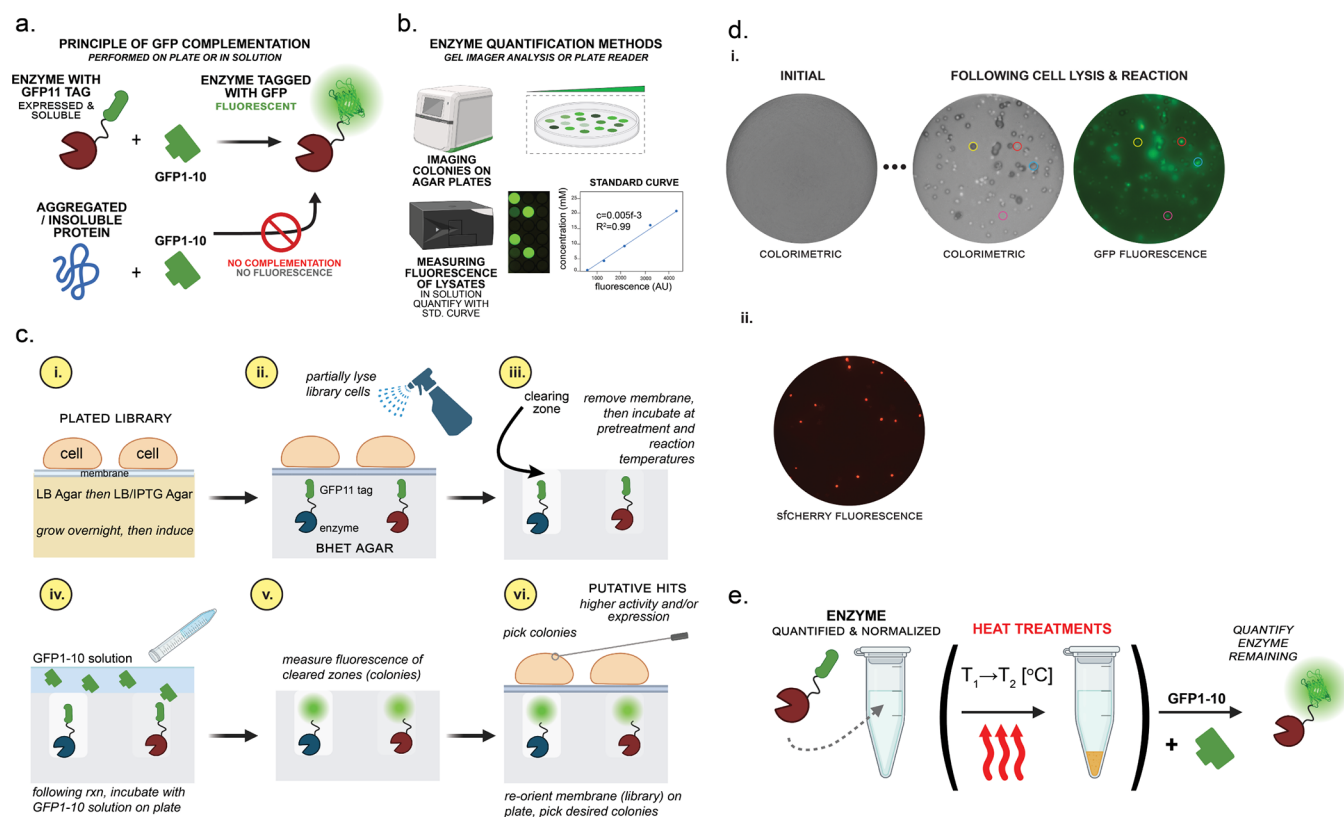
Figure 2. HT coscreening assay for screening PET hydrolase libraries. a. Principle of split GFP complementation. Soluble, highly expressed enzymes (tagged with GFP11), when complemented with GFP1−10, yielded a fluorescent signal, while aggregated, insoluble, or poorly expressed enzymes showed little to no fluorescent signal upon complementation. b. Enzyme quantification using split GFP. On plates, a gel imager with fluorescence detection (or other camera with fluorescence detection) visualized the amount of enzyme expressed via GFP complementation after cell lysis. Relative GFP fluorescence gave a qualitative comparison of the soluble enzyme amount expressed. In solution, a plate reader measured enzyme expression in cell lysates in microwell plate formats. Enzymes in lysates were then quantified by using a standard curve of a known protein with known concentrations. c. Co-screening of enzyme activity, expression, and solubility levels via BHET screening plates and GFP complementation. (i) The *E. coli* library was plated on a semipermeable membrane and grown overnight on LB agar plates, then induced by moving the membrane to an LB agar plate with IPTG. (ii) The membrane was then moved to the BHET agar screening plate and partially lysed, allowing enzymes (tagged with GFP11) to diffuse into the BHET agar plate. (iii) During incubation at the reaction temperature (following heat treatment at a higher temperature), clearing zones began to appear, indicating hydrolysis of the BHET model substrate. (iv) Following the reaction, GFP1−10 was added to the plates and incubated to complement the GFP11 of the enzymes. (v) Fluorescence zones appeared as functional GFP associated. (vi) Colonies with improved solubility and/or activity were chosen based on fluorescence and colorimetric (clearing zones) assays after the membrane was reoriented on the plates. d. Snapshots of a plate showing how the coscreening assay was done for a small portion of the LCC library. (i) A BHET agar plate was shown initially as opaque. After incubation with colony lysates, clearing zones (halos) began to appear (detected by colorimetric blot). Following the reaction, GFP1−10 complementation yielded a green fluorescence signal proportional to the amount of enzyme released from each partially lysed colony. Here, the yellow-circled colony showed high activity/low solubility; the blue-circled colony showed high activity/high solubility; the red-circled colony showed low activity/high solubility; the pink-circled colony showed low activity/low solubility. (ii) Cells expressing sfCherry in pET21b(+) were seeded into libraries, plated, and lysed along with the enzyme library. Approximate equal fluorescence indicates colonies were homogeneously lysed across plates. Images were taken with a Bio-Rad ChemiDoc MP with colorimetric blot, Alexa 488 (green; GFP), and Alexa 546 (red; sfCherry) analysis. e. A schematic illustration of how split GFP complementation was used to measure enzyme thermostability in cell lysates by quantifying the enzyme amount in samples before and after heat treatments at various temperatures.

GFP reassembled to generate green fluorescence, which was directly correlated to the concentration of enzyme present (brighter green fluorescence corresponded to higher enzyme concentration). Enzyme libraries were additionally coscreened for activity on BHET agar plates based on clearing zones (halo) generated from BHET hydrolysis (Figure 2c). We hypothesized that an enzyme with high activity on BHET would have high activity on PET, so prior to testing on PET substrates (which is more difficult to set up in HT assays), we were able to select for high-performing variants using this model substrate.

As shown in Figure 2c, enzyme libraries were first grown on semipermeable membranes on LB agar plates overnight and then expressed by transferring the membranes to plates containing IPTG for induction. Membranes were then moved to BHET agar screening plates, colonies were partially lysed by spraying with BugBuster, allowing the cell lysates to diffuse through the membranes onto the BHET agar plates, and membranes were finally returned to LB agar plates and stored at 4 °C for later colony picking. The BHET agar plates were then incubated at reaction temperature (65−70 °C) for 5 to 20 h. Coupling the BHET hydrolysis reactions and split GFP complementation assays allowed us to quickly and precisely select colonies that exhibited higher enzyme activity (larger clearing zones or larger halo) and/or better expression levels (higher fluorescence intensities) by aligning BHET

screening plates to the original colonies grown on the membranes, allowing for colonies to be picked (Figure 2c,d). Selected colonies were prelabeled on the BHET agar plates by analyzing the images of BHET agar plates taken with a Bio-Rad ChemiDoc MP under colorimetric blot and Alexa 488 detection settings for larger clearing zones and/or brighter green fluorescence intensities (Figure 2d). BHET hydrolysis was stopped by storing BHET screening plates at 4 °C until ready for colony picking.

Coarse screening was first performed on individual colonies from plated libraries ($\sim 2 \times 10^3$ colonies/single plates, Figure S1), and then colonies were selected based on qualitative analysis of larger clearing zones and/or brighter green fluorescence intensities. The colony size and number were controlled via proper cell stock dilution and growth conditions (see the Methods section). The enzyme variants selected from coarse screening were then validated and further screened in a fine screening assay as described above (for both split GFP complementation and BHET hydrolysis), except that cell cultures were now grown in 96-well plate formats ($\sim 10^2$) alongside cells expressing a starting enzyme and/or LCC-ICCG and stamped on a membrane using a replicator tool (Figure 1). In the fine screening assay, colony sizes were bigger, ~ 2 mm in diameter, as a result of being replicated from a 96-well plate cell culture by a replicator tool. For each 96-well plate of colonies picked from the coarse screening, BHET hydrolysis was evaluated on two BHET agar plates at the reaction temperature, one at the same concentration that was used for the coarse screening assay, and the other at an increased BHET concentration (20−40 mM higher concentration than on the coarse screening plates) and incubated for a longer reaction time (up to 48 h) to ensure that thermostability properties were interrogated during the selection process. BHET hydrolysis was monitored by taking images of the BHET agar plates with a Bio-Rad ChemiDoc MP under colorimetric blot every hour after incubation for the first 6 h and then for 15 h, 24 h, 36 h, and up to 48 h. Enzyme variants that displayed increasingly higher BHET hydrolysis (larger clearing zones) throughout the reaction time compared to starting templates were selected as putative hits for activity validation on actual PET substrates.

In addition, enzyme libraries on BHET agar plates were also screened for thermostability properties by pretreatment of BHET agar plates at elevated temperatures: 80 °C prior to BHET hydrolysis reactions. Throughout the directed evolution process, different selection pressures were implemented after each round of evolution, including a) increasing BHET concentrations (starting at 20 mM and gradually increasing up to 120 mM); b) increasing reaction temperatures (starting at 65 °C and then increasing to 70 °C) and reaction duration (starting at 5 h and gradually increasing up to 48 h); c) performing preheat treatment at 80 °C before the enzyme reaction on BHET plates. Increasing intensities of selection pressures after each round of evolution, such as using higher BHET concentrations and higher reaction temperatures, were implemented to select for enzymes with enhanced catalytic conversion at higher substrate concentrations near 70 °C.

Screening and Validation of Putative Hits' Catalytic Performance on PET Substrates. Improved enzyme variants ($\sim 10^1-10^2$) selected from the above HT coscreening assay were next evaluated for catalytic performance on either amorphous PET film coupons or high-crystallinity PET powder (Figure 1c). Enzymes were expressed on a small scale (1 to 5 mL cell culture) and were quantified via split GFP fluorescence with cell lysates, using a standard curve of fluorescence intensity of a standard protein (sulfite reductase) expressed with GFP11[44] at known concentrations. Enzyme concentrations in cell lysates were normalized to 1 μM and diluted 10-fold in reactions (0.1 μM enzyme; 500 μL reactions) with amorphous PET film coupons or high-crystallinity PET powder in microwell plates. Activity, measured as total aromatic products, was monitored over time by UV absorbance.[33,34] Enzyme thermostability was measured for cell lysates by quantifying the enzyme amount in samples before and after heat treatments (after being centrifuged to separate any debris) at various temperatures using the split GFP complementation assay (Figure 2e). Identified improved enzyme variants were then used as parents for the next round of directed evolution or, if determined to have met the desired engineering goals, were expressed, purified, and more thoroughly characterized using HPLC and pH-controlled bioreactors.

Engineering LCC Using Our HT Screening Platform. We sought to demonstrate the efficiency of our newly developed platform to improve the catalytic efficiency of a benchmark PET hydrolase, LCC-ICCG.[17,47] Directed evolution was first initiated using wild-type LCC (LCC-WT) as the starting template. Libraries of DNA fragments containing random mutations were created using DNA shuffling, cloned into the pET21b(+)-GFP11 screening vector with a C-terminal GFP11 tag, and transformed into *E. coli*. Enzyme libraries were then screened using the HT coscreening assay, first with coarse screening, followed by fine screening. In the first round, the library was screened on 20 mM BHET agar plates at 65 °C after 5 h of reaction. Putative hits were selected after fine screening on BHET agar plates at 20 and 40 mM concentrations at 65 °C, up to 24 h of reaction time. Selected enzyme variants from the first round mostly contained single mutations, including P38L, V118I, and L159Q, that displayed higher activity (larger clearing zones) on BHET agar plates compared to LCC-WT. These variants were then pooled together as parents for the second round of directed evolution, with the coarse screening assay done at an increased BHET concentration (40 mM) and increased temperature (68 °C) for a longer reaction time (7 h), and the fine screening assay performed on 40 and 60 mM BHET agar plates at 68 °C and monitored up to 24 h of reaction time. After two rounds of directed evolution, we obtained a variant, LCC-F2, with mutations V118I, A149V, L159E, and V202I, that exhibited higher activity compared with LCC-WT and comparable enzyme solubility/concentration on BHET agar plates. Validation assays, performed using enzymes in cell lysates normalized to a final concentration of 0.1 μM, showed that LCC-F2 had $\sim 13\%$ higher activity toward high-crystallinity PET powder compared to LCC-WT after 6 h of reaction (Figure S2a,e). However, this variant showed $\sim 23\%$ lower activity compared to LCC-ICCG on the same substrate (Figure S2a,e); thus, we continued with additional rounds of directed evolution.

The addition of a disulfide bond in LCC-WT (D238C−S283C) was found to increase enzyme thermostability, as previously reported.[23] To improve LCC-F2's performance, we constructed the same disulfide bond by adding it to the LCC-F2 and LCC-P38L variants and included LCC-ICCG as one of the starting scaffolds shuffled in the next round of directed evolution. After the third round of evolution (coarse screening
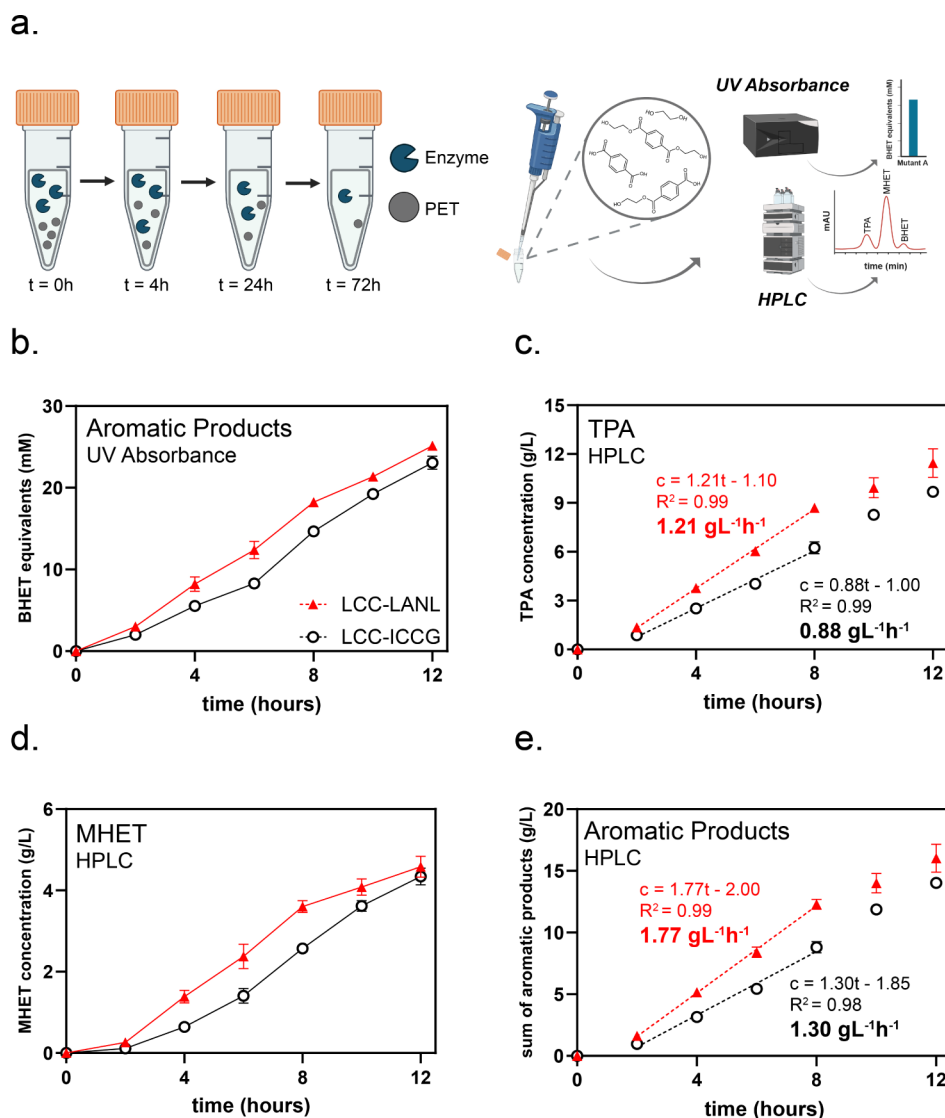
Figure 3. PET hydrolysis was performed by LCC-LANL and LCC-ICCG. a. Analysis workflow was performed for PET hydrolysis over time. Enzymes were incubated with amorphous PET coupons (3 mm circles, 0.25 mm thick, and 2.5 mg each), with samples taken over time, to measure aromatic product release. Products were quantified either by UV absorbance, to measure aggregate soluble aromatic products, or by HPLC, to quantify monomers TPA, MHET, and BHET. b. PET deconstruction was performed by engineered LCC-LANL (red triangles) and LCC-ICCG (white circles), with UV absorbance analysis. Aggregate product concentration as BHET equivalents is shown for time points taken over 12 h with purified enzymes (0.7 mg of enzyme/g of PET) with 2.9% (w/v) PET film coupons at 68 °C in 100 mM sodium phosphate buffer, pH 8. HPLC analysis of the reaction quantifying the c. TPA concentration, d. MHET concentration, and e. sum of aromatic products. Best-fit lines (equations and R^2 values shown) are shown as dotted lines 2 to 8 h. Data points show the average of $n = 3$ replicates, with error bars ± 1 S.D; p-values for different slopes are all <0.0001.

was performed on 60 mM BHET agar plates and at a reaction temperature of 70 °C for 20 h, with subsequent fine screening performed on 60 mM and 80 mM BHET agar plates at 70 °C for 48 h), a variant, LCC-F6, containing mutations P38L, L117P, and A149V, in addition to the LCC-ICCG mutations (Y127G, D238C, F243I, and S283C), was selected, as it displayed comparable activity to LCC-ICCG on both amorphous PET film coupons and high-crystallinity PET powder substrates after 6 h of reaction at 70 °C (Figure S2b,c,e). This variant also has a similar expression and solubility level compared to LCC-ICCG.

At this point, our goal was to engineer new LCC variants with enhanced hydrolysis performance on amorphous PET coupons (ubiquitous in lab-scale PET hydrolase testing[16,17,19,21]), relative to the benchmark LCC-ICCG. Using

LCC-F6 as a template, the next, fourth round of directed evolution was performed on 80 mM BHET agar plates at 70 °C for 20 h, with fine screening validated on both 80 mM and 100 mM BHET agar plates at 70 °C for 48 h. This evolution round yielded the top two variants: LCC-B8 and LCC-C9. In addition to the mutations present in the LCC-ICCG parent (Y127G, D238C, F243I, and S283C), LCC-B8 contained mutations P38L, L117P, A149V, and S247L, and LCC-C9 contained mutations P38L, Y61C, M91I, L117P, A149V, and S247L. After 6 h of reaction with amorphous PET film coupons at 70 °C, LCC-B8 displayed a 5.2-fold higher aromatic product release and a 5.6-fold higher maximal rate compared to LCC-ICCG, while LCC-C9 had about an 11-fold higher aromatic product release and a 10.6-fold higher maximal rate (Figure S2c,e). The two variants, however, displayed lower

activities on high-crystallinity PET powder, with ∼16 and 22% less aromatic products compared to LCC-ICCG, respectively (Figure S2b,e). These two variants, LCC-B8 and LCC-C9, were pooled together, and one more round of directed evolution was performed.

To select for enhanced thermostability properties of the new enzyme variants, a preheat treatment step at 80 °C for 1 h was implemented prior to the BHET hydrolysis reaction at 70 °C. BHET concentrations were also increased to 90 and 120 mM with longer reaction times of 20 h and up to 48 h for the coarse screening and the fine screening assays, respectively. The fifth round of directed evolution yielded the top variant, LCC-LANL (after Los Alamos National Laboratory), displaying a 14.3-fold higher aromatic product release and a 13.9-fold higher maximal rate compared to LCC-ICCG after 6 h of reaction with amorphous PET film coupons at 70 °C (Figure S2d,e). This variant, LCC-LANL, was therefore selected for final characterization after being expressed and purified from 1 L of cell culture (Figure S3). LCC-LANL contained nine mutations: P38L, Y61C, M91I, L117P, A149V, H218Y, Q224H, S247L, and T256I, in addition to those present in the the LCC-ICCG scaffold (Y127G, D238C, F243I, and S283C). The DNA and amino acid sequences of LCC-WT, LCC-F2, LCC-F6, LCC-B8, LCC-C9, LCC-LANL, and LCC-ICCG are shown in Tables S1 and S2, respectively. A table summarizing the best variants obtained from each round of directed evolution, along with their performance compared to LCC-WT or LCC-ICCG, is shown in Figure S2e, and a map of the evolutionary trajectory of the final variant LCC-LANL is shown in Figure S2f. A BHET agar plate obtained from the fine screening showing a comparison of the BHET hydrolysis clearing zones of LCC-B8 against those of LCC-ICCG is shown in Figure S2g.

Characterization of LCC-LANL. Following testing to characterize the evolved, purified enzyme, LCC-LANL, we compared its performance to that of the benchmark and parent, LCC-ICCG. We found that LCC-LANL had an increased maximal catalytic rate compared to the parent enzyme, LCC-ICCG, in the hydrolysis of amorphous PET film coupons at 68 °C ($p < 0.0001$, for both TPA and the sum of aromatic products) (Figure 3). Analysis was performed with UV absorbance and HPLC aromatic monomer quantification (Figure 3a), with the two methods giving similar results (Figure 3b−e). LCC-LANL showed an initial rate of 1.21 g L^{-1} h^{-1} TPA and 1.77 g L^{-1} h^{-1} aromatic products, compared to 0.88 g L^{-1} h^{-1} TPA and 1.30 g L^{-1} h^{-1} aromatic products for LCC-ICCG (Figure 3c,e). Product ratios for both enzymes were approximately equal to and constant over time (about 70% TPA) (Figure 3c,d).

While initial reactions were performed under the conditions at which LCC-ICCG was reported to have the highest activity (68 °C, 100 mM phosphate buffer, pH 8, with amorphous PET film),[17,47] we chose to further evaluate LCC-LANL (and LCC-ICCG) at different temperatures and for longer reaction times, beyond the initial periods used to measure the maximum rates. Therefore, LCC-LANL and LCC-ICCG were additionally tested at 65 °C (Figure S4a−d) and 70 °C (Figure S4e−h).[17,47] Similar to the results at 68 °C, we observed that LCC-LANL exhibited a higher maximal rate than LCC-ICCG at 65 °C ($p < 0.0001$, for both TPA and the sum of aromatic products) (Figure S4a−d), with similar results between UV absorbance measurements and HPLC monomer quantification. However, at 70 °C, LCC-LANL showed a statistically

insignificant increase in the maximal hydrolysis rate compared to LCC-ICCG ($p = 0.0904$ for TPA; $p = 0.4077$ for the sum of aromatic products) and with diminishing activity beginning after 8 h of incubation (Figure S4e−h). The increase in product release and maximal rates for LCC-LANL vs LCC-ICCG, however, was not as large when using purified proteins as when using crude cell lysates with the same enzyme concentrations (normalized based on split GFP complementation as discussed in the Methods section) (Figure S2d).

Upon looking at hydrolysis activities up to 24 h (Figure S5), we saw similar diminished activity at 12 h or earlier for LCC-LANL, while LCC-ICCG continued to show depolymerization continuing to 24 h. At 65 and 68 °C, however, further activity increases by LCC-ICCG (post-24 h) did not result in substantially more total product release than LCC-LANL, only 11 and 8% higher at 65 and 68 °C, respectively (Figure S5d,h). We also observed that the ratio of TPA over MHET released for LCC-LANL was higher than that of LCC-ICCG at both the 12 and 24 h time points (Table S3). Despite its significantly increased maximal rate compared to LCC-ICCG, our variant, LCC-LANL, seemed to plateau in activity by 12 h. Decreased thermostability or product inhibition were possible explanations. In screening for LCC-LANL variants, heat treatment at 80 °C for 1 h was implemented as a selection pressure to maintain the high thermostability of LCC-ICCG ($T_m = 94.5$ °C),[17] and LCC-ICCG was demonstrated to not experience product inhibition.[17] Still, to fully determine the extent and potential effects of decreased thermostability in LCC-LANL, we conducted further experiments.

Differential scanning calorimetry analysis (Figure S6) revealed that the thermal unfolding of each enzyme is essentially an irreversible process, with LCC-LANL and LCC-ICCG exhibiting comparable energy barriers (E_{act}) to unfolding from the native to denatured state. However, LCC-LANL can overcome this energy barrier with a given frequency (1 s^{-1}) at a temperature (T_{act}) of approximately 10 °C lower than LCC-ICCG, and hence, has kinetic stability lower than that of the latter variant. Notwithstanding this property, evaluating the thermostability of LCC-LANL using the split GFP complementation assay (Figure 2e), we observed that, while the LCC-LANL enzyme experienced decreased survivability above 72 °C, at lower temperatures, LCC-LANL showed similar thermostability as LCC-ICCG, with essentially 100% protein being retained after heat treatment at 72 °C for both proteins (Figure S7).

In order to evaluate LCC-LANL's performance on the various PET substrates that these enzymes would likely encounter in industrial applications,[47−49] we next sought to evaluate the hydrolytic activity of LCC-LANL on alternative forms of PET, namely, milled amorphous PET film and high-crystallinity PET powders (purchased from Goodfellow, 41.8% crystallinity;[50] see the Methods section).

On the amorphous PET powder substrate (Figure S8), it was observed that the maximal rates of LCC-LANL and LCC-ICCG exceeded those observed for amorphous PET films (as coupons, i.e., unmilled). This trend persisted across all three reaction temperatures (Figures 3b−e, S4, and S8). In addition, a noteworthy observation was a shortened lag period for the powder substrates, with maximal rates occurring within 2 h. However, activity appeared to plateau for powder substrates by both LCC-LANL and LCC-ICCG, with lower total hydrolysis over shorter (Figures 3b−e, S4, and S8) and longer (Figures S5 and S9) reaction times. Additionally, we did not observe the
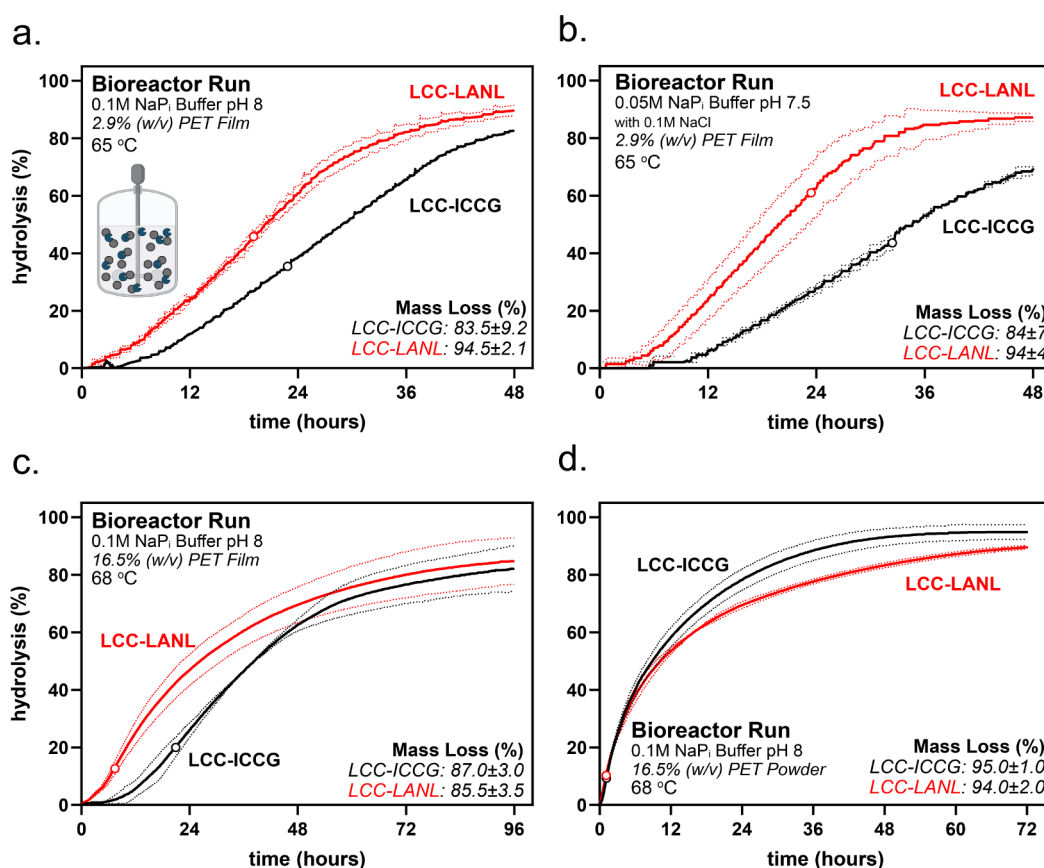
Figure 4. PET hydrolysis by LCC-LANL and LCC-ICCG in pH-controlled bioreactors. Enzymes LCC-ICCG (black) and LCC-LANL (red) were added to reactions of PET coupons (2.9 or 16.5% (w/v)) in 100 mL bioreactors. Enzyme loading was 0.7 mg/g for 2.9% (w/v) PET and 1 mg/g for 16.5% (w/v) PET. Bioreactors were monitored for the hydrolysis of PET, with total mass loss observed after the end of the reaction. Reactions were stirred at 400 rpm, with a. 100 mM sodium phosphate pH 8 reaction buffer at 65 °C with 2.9% amorphous PET film coupons, b. 50 mM sodium phosphate buffer pH 7.5 with 100 mM NaCl at 65 °C with 2.9% amorphous PET film coupons, c. 100 mM sodium phosphate pH 8 reaction buffer at 68 °C with 16.5% amorphous PET film coupons, or d. 100 mM sodium phosphate pH 8 reaction buffer at 68 °C with 16.5% amorphous PET powder. Data points show the average of $n = 2$ bioreactors, while dotted lines represent ± 1 SD. For each profile, a circle marks the center of the 3 h window exhibiting the highest hydrolysis rate.

same significant increases in the maximal hydrolysis rate for amorphous PET powders as we did with films for LCC-LANL compared to LCC-ICCG (for the sum of aromatic products: 65 °C, $p = 0.0127$; 68 °C, $p = 0.190$; 70 °C, $p = 0.1345$). While at 65 °C, we observed approximately 2-fold increases in the rate for LCC-LANL over LCC-ICCG, the rates at 68 and 70 °C (the regime at which LCC-ICCG was reported to have the highest activities) were not significantly increased for LCC-LANL (Figure S8). The ratio of TPA over MHET released for LCC-LANL, however, was higher than that of LCC-ICCG at both the 12 and 24 h time points (Table S3).

In reactions with high-crystallinity PET powder, maximal rates (Figure S10) and total hydrolysis over time (Figure S11) were largely reduced compared to the other amorphous PET substrates, and no significant improvement in maximal rates was observed for LCC-LANL over LCC-ICCG (for the sum of aromatic products: 65 °C, $p = 0.0961$; 68 °C, $p = 0.5053$; 70 °C, $p = 0.5866$), as well as no lag period, with maximal rates occurring within 2 h. The hydrolysis rates of LCC-LANL and LCC-ICCG were comparable up to 12 h at all temperatures, although LCC-ICCG appeared to outcompete LCC-LANL by 24 h, with approximately 50% higher activities. This result was expected because amorphous PET film coupons (not high-crystallinity PET powder) were used as the main substrates

screened in our validation assays to select for enzyme variants with enhanced hydrolysis performance on amorphous PET film coupons, as indicated in our engineering goals. Notably, similar to what was observed in reactions with amorphous PET substrate, the ratio of TPA over MHET released in reactions with high-crystallinity PET powder for LCC-LANL was higher than that of LCC-ICCG measured at both time points (Table S3).

To further evaluate the performance of our variant, we tested LCC-LANL and LCC-ICCG in pH-controlled bioreactors, under the same conditions as the small-scale experiments indicated above: 100 mM sodium phosphate buffer, pH 8, 2.9% (w/v) PET, and 0.7 mg of enzyme/g of PET at 65 °C (Figure 4a). We observed that LCC-LANL outperformed LCC-ICCG in depolymerization of amorphous PET film coupons. Both enzyme variants exhibited a lag before their maximum substrate hydrolysis rate was attained, a phenomenon previously reported for hydrolysis of amorphous PET film by LCC variants.[51] Notably, LCC-LANL showed a 38% higher maximal rate than LCC-ICCG and near-complete conversion of PET to hydrolytic products, with approximately 24% hydrolysis in 12 h, compared to 12% by LCC-ICCG, and over 80% hydrolysis by 36 h, compared to approximately 65% by LCC-ICCG. By the end of the 2-day reaction, LCC-LANL

achieved 94.5% polymer mass loss (see the Methods section), compared to 83.5% by LCC-ICCG. It is likely that the new mutations in the LCC-LANL construct change the pH optimum of the enzyme, making it less capable of tolerating the acidification due to TPA accumulation in small-scale, batch reactions; however, such conditions were eliminated in the bioreactor experiments.

To test our enzyme variant performance under alternate, more industrially relevant conditions, requiring fewer buffer constraints and reaction at lower pH, both of which would contribute to improved process economics,[49,52] LCC-LANL was compared to LCC-ICCG in pH-controlled bioreactors at 50 mM sodium phosphate buffer, pH 7.5 with 100 mM NaCl, 2.9% (w/v) PET, and 0.7 mg of enzyme/g of PET at 65 °C (Figure 4b). Similar to the previous experiment, LCC-LANL showed higher performance compared to LCC-ICCG, with a 9% higher maximal hydrolysis rate vs the parent, and a significantly improved hydrolysis profile. LCC-LANL showed approximately 24% hydrolysis in 12 h, compared to 6% by LCC-ICCG, and over 80% hydrolysis by 36 h, compared to only about 50% by LCC-ICCG in 36 h. The mass losses were comparable to the original conditions, with 94% mass loss by 48 h by LCC-LANL and 84% by LCC-ICCG.

High PET solid loadings are necessary to ensure optimal productivity (i.e., high product yield) of PET degradation reactions.[47,52] We, therefore, performed additional bioreactor runs at 68 °C with increased PET loadings, 16.5% (w/v) (based on a recently reported guideline,[47] either as amorphous PET film coupons or milled amorphous PET powder (with enzyme loading at 1 mg/g of PET). With amorphous PET film coupons at this substrate loading, LCC-LANL maintained improved performance compared to LCC-ICCG, with a 43% higher maximal rate (that occurred 13 h sooner, demonstrating a shortened lag period), nearly twice the conversion after 24 h, and a higher extent of hydrolysis up to 48 h. However, both LCC-LANL and LCC-ICCG yielded similar mass losses and hydrolysis extents by 72 h and up to 96 h at 68 °C (Figure 4c).

Milling the amorphous PET coupons to a powder appeared to eliminate the lag period for both enzymes and increased extents of hydrolysis and total mass loss by roughly 10% by 72 h. Additionally, in this reaction, with 16.5% amorphous PET powder, LCC-ICCG outcompeted LCC-LANL by up to 12% (occurring at ~33 h) (Figure 4d). However, maximal rates and total mass loss were comparable for both enzymes. Specifically, LCC-ICCG had an 8% higher maximal rate, with both enzymes reaching this at ~1.5 h. Both LCC-ICCG and LCC-LANL yielded similar mass losses and hydrolysis extents by 72 h at 68 °C. Notably, cryo-milling amorphous PET film coupons to powder appeared to increase PET crystallinity from 9.4 to 13%, as determined by differential scanning calorimetry (DSC) (Figure S12). While the engineering goal was to develop enzymes with enhanced hydrolysis of amorphous PET film coupons here, we posit that eliminating the need for substrate pretreatment (i.e., milling) could be a promising route to improving process economics,[52] while only taking a meager reduction in overall enzyme performance.

Structural Analysis of LCC-LANL. The structure of LCC-LANL was modeled using the Rosetta macromolecular modeling suite.[53] Most of the mutations obtained from directed evolution led to increased solvent-exposed hydrophobicity. The S247L mutation particularly was shown to increase the hydrophobic surface area near the active site of the enzyme (Figure 5a,b). While this could destabilize the protein
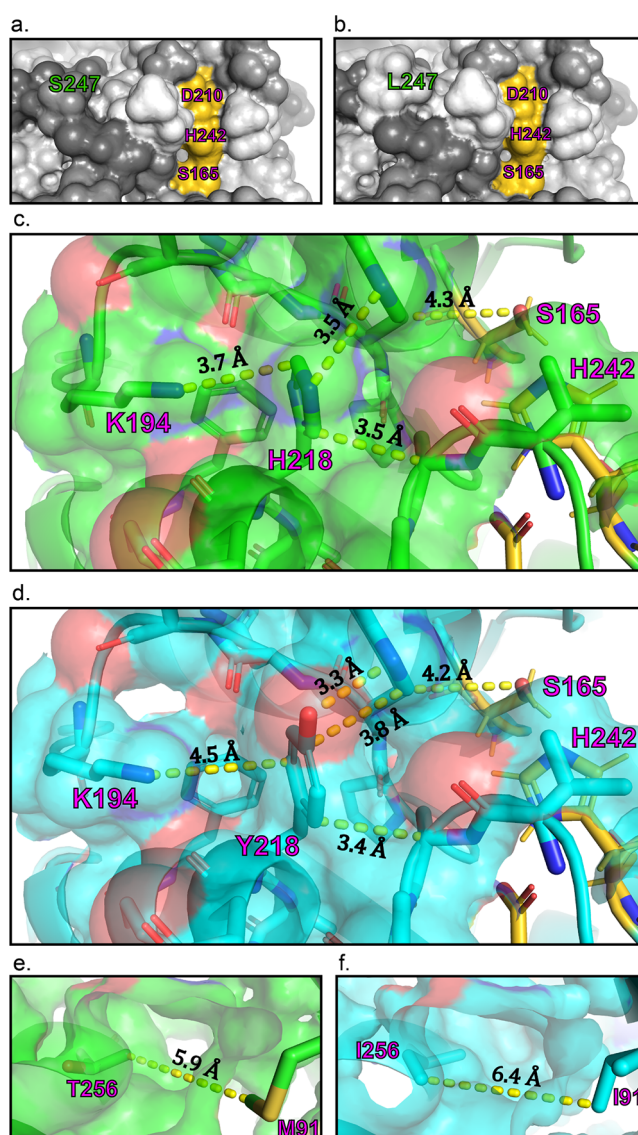

Figure 5. Structural analysis and comparison of mutation sites in LCC-LANL, with respect to LCC-ICCG. a. Surface hydrophobicity rendering for the LCC-ICCG active site (yellow shading) with S247 labeled. b. Surface hydrophobicity rendering for the LCC-LANL active site with L247 labeled. The lighter gray color indicates higher hydrophobicity near the active site in LCC-LANL. c. Packing of K194 and H218 in LCC-ICCG. d. Packing of K194 and Y218 in LCC-LANL. The H218Y mutation in LCC-LANL improved packing by establishing close to ideal geometry for a canonical cation−pi interaction. e. Packing around M91 and T256 in LCC-ICCG. f. Packing around I91 and I256 in LCC-LANL. In panels c−f, carbon atoms are colored green for LCC-ICCG and cyan for LCC-LANL. Other atoms maintain Corey−Pauling−Koltun (CPK) coloring. Mutated residues are labeled in pink. Side chain residues are shown as sticks, with a translucent overlay of the Connolly molecular surface.

structure, it may be favorable in the presence of a substrate, which is primarily hydrophobic. The H218Y mutation (Figure 5c,d), also observed by Cribari et al.,[43] was found to add hydrophilic surface area to the enzyme and may help with protein stability. This mutation also improved surface packing by reducing exposed hydrophobic surface area, establishing a near-ideal cation−pi interaction geometry and thereby removed a potential site for nonproductive PET binding. In addition, this mutation removed a titratable and strong

charge−charge repulsion interaction between H218 and K194, given their tight packing. Indeed, the distance between K194 and H218 was found to increase by 0.4 Å (Figure S13a,b), compared to the original solved structure (PDB: 8JMP) upon running the Rosetta Relax energy minimization program. The predicted configuration of K194 in LCC-LANL may also allow for better solvation, which is likely for lysine, one of the most hydrophilic residues and not participating in an ion pair interaction. Additional results of structure refinement using Rosetta Relax are shown in Figure S13c−f.

The remainder of the mutations were farther from the active site. Among these, the M91I and T256I mutations (Figure 5e,f) may be synergistic in establishing a more uniformly hydrophobic core, although with the creation of several voids. These may lead to increased mobility and therefore increased catalytic efficiency of the LCC-LANL enzyme at lower temperatures, 65 °C, compared to 68 and 70 °C. However, the voids may also decrease thermostability. The L117P mutation was predicted to be destabilizing, as it removed backbone hydrogen bonding and created cavities in the protein core directly and through lever-arm effects on the backbone (details in Table S4). These may be worthwhile target sites to evolve in continued evolution cycles on the LCC-LANL template.

Conformational ensembles of the individual mutations, the LCC-LANL mutant, and the LCC-ICCG mutant produced contrasting predictions for stability. The Rosetta score distributions for these models are shown in Figure S14. An analysis of LCC-LANL individual mutations and how these mutations may affect the enzyme from a structural perspective is provided in Table S4.

Molecular Docking of PET to LCC-ICCG and LCC-LANL. Flexible ligand docking simulations revealed several stable nonproductive binding modes for the PET substrate near the active site of LCC-ICCG. Out of the 100 predicted best binding modes, 60 were productive, having substrate atoms within 4 Å of the catalytic residues, S165, D210, and H242. Notably, all 100 predicted best binding modes were productive for LCC-LANL. The Rosetta scores, as well as its component terms, were statistically analyzed for these modes and the entire ensemble. The analyses revealed that the difference in the total Rosetta score (total_score) between the docked and free states was higher for LCC-LANL than for LCC-ICCG (Table S5). This suggests that LCC-LANL is stabilized from binding to PET more than LCC-ICCG. The greater stabilization upon binding to PET may manifest in higher binding affinity, which may explain the higher catalytic efficiency observed in bioreactor experiments with amorphous PET film coupons. This may also explain the differences in the maximal rates of LCC-LANL vs LCC-ICCG in cell lysates compared to purified protein samples due to more unspecific binding in cell lysates, which may have resulted in more frequent binding of LCC-LANL to PET film coupons than LCC-ICCG. The same trend, however, was not observed for amorphous PET powder, potentially because of surface structures and charges changing and increased crystallinity upon being milled. More detailed studies on LCC-LANL's interaction with this substrate type may provide valuable insights into how LCC-LANL was conferred with higher hydrolytic activity on amorphous films but not powders.

Discussion and Conclusions. In this study, we developed an integrated platform that enables efficient engineering of PET hydrolases by directed evolution with random muta-

genesis by coupling split GFP complementation and BHET model substrate activity assays. We found that enzyme variants with higher hydrolytic activity in the BHET model substrate assay generally had higher maximal rates on amorphous PET film coupons. However, their activity could potentially plateau quickly on PET, and thus a validation assay on actual PET substrates is needed to be performed to select for enzyme variants that not only had higher maximal rates but also retained high catalytic activity over time. This screening platform could be a useful tool for PET hydrolase engineering, allowing the measurement of specific protein activity and thermostability prior to protein purification, thereby enabling the rapid selection of improved enzyme variants. We then demonstrated the utility of this platform to discover new mutations enhancing the maximal rate of a benchmark PET hydrolase, LCC-ICCG, on amorphous PET film coupons. The engineered enzyme, LCC-LANL, met the desired engineering goal by displaying a higher maximal rate than the parent, LCC-ICCG, on amorphous PET film coupons. LCC-LANL also outperformed this benchmark in large-scale, pH-controlled bioreactors, in deconstructing amorphous PET film coupons at both 65 and 68 °C, up to 48 h. However, both LCC-LANL and LCC-ICCG appeared to have similar catalytic activity over an entire 96 h reaction on amorphous PET film. This is likely due to the screening conditions that were employed when testing our platform (selecting for improved enzyme variants in up to 48 h of reactions with BHET in fine screening assays and using amorphous PET film as the main substrate to validate the activity of enzyme variants in validation assays), which were set up based on the goal to engineer new LCC variants with enhanced hydrolysis performance on amorphous PET coupons.

The platform developed here can screen $\sim 10^4$ or more colonies in $\sim 2-3$ days and is readily scalable. In addition, this platform uses only widely accessible reagents and equipment with ease-of-use and low chemical hazards, allowing it to be easily and readily adopted by researchers worldwide. We anticipate that this new platform will relieve a major bottleneck in PET hydrolase engineering by not only simultaneously screening for enzyme expression, solubility, and catalytic activity near T_{opt} but also allowing the efficient screening of large, diverse libraries. We anticipate more accelerated directed evolution of these high-performance enzymes, providing pathways toward meeting goals informed by process modeling[49,52] to improve enzymatic PET recycling. Beyond this work, the platform is adaptable to a variety of PET hydrolase engineering applications, including reaction temperatures, pH, buffer conditions, use of alternative substrates, higher substrate crystallinities, and the presence of any dyes or other additives that may pose an inhibitory effect to enzymatic activity by changing selection pressures. Improved enzyme performance under these conditions may alleviate major cost and environmental impact drivers currently hindering industrial enzymatic PET recycling.[49,52]

While the platform described here may be useful for discovering novel BHET hydrolases[54] from metagenomic libraries, it is, however, not yet optimized to discover novel PET hydrolases without additional screening steps, as high BHET hydrolysis may lead to the discovery of enzyme groups that break down short esters but not polyesters. In addition, the use of BHET in our HT screening assay may not yet be optimized to distinguish enzymes with only slightly higher degradation activity on PET. Therefore, a validation assay on

actual PET substrates is always needed to select for enzyme variants that depolymerize PET or confirm whether they have higher PET hydrolase activity. Alternatively, BHET could be used as a model substrate in the coarse screening to enable colony-level screening and selection in a high-throughput format, followed by PET nanoparticles[19,29] as substrates in the fine screening, where a higher concentration of cells could release a higher amount of enzymes, thus permitting the detection of PET depolymerization activity via change in turbidity. The HT screening assay reported here was performed qualitatively to quickly select for enzyme variants with improved enzyme expression, solubility, and catalytic activity based on green fluorescent signals and halo sizes. In the future, further refinement could be made to directly calculate a semiquantitative specific activity of improved enzyme variants based on halo sizes and green fluorescent signals, with respect to the starting enzyme templates.

Further engineering of LCC could be pursued, including combining activity-improving variants with mutations that confer higher thermostability[55] to create an enzyme with superior maximal rates and enhanced activity over long reaction times, exploring optimal residues at mutation sites of LCC-LANL, or engineering new LCC variants with improved activity toward high-crystallinity PET substrates. Further characterization of LCC-LANL, both biophysically, and through testing with a broader suite of varied reaction conditions (i.e., pH, temperature, and PET substrate types) will better allow us to determine and further evaluate how this variant has been conferred with improved depolymerization properties, as well as to optimize reaction conditions for maximal PET deconstruction. LCC-LANL was demonstrated to be efficient in breaking down amorphous PET film coupons (which are ubiquitous in lab-scale PET hydrolase engineering), underscoring the potential of this newly developed platform for PET hydrolase engineering.

■ METHODS

Materials and Data Analysis. Unless otherwise noted, materials were purchased from the following vendors. Oligonucleotides were purchased from Integrated DNA Technologies. Genes were synthesized by Twist Biosciences. Sanger sequencing was performed by Genewiz. Enzymes were purchased from New England Biolabs. Amorphous PET films (product #ES301445; 9.4% crystallinity) and high-crystallinity PET powder (product #ES306031; 41.8% crystallinity)[50] were purchased from Goodfellow Cambridge Ltd. Chemicals were purchased from Fisher Scientific or Millipore Sigma. Kits were purchased from Qiagen. Data analysis and curation were performed in Microsoft Excel, GraphPad Prism, and Agilent OpenLab CDS. Sequencing and gene design were performed using ApE (M. Wayne Davis) and SnapGene (Dotmatics). Figures were prepared with Adobe Illustrator and BioRender.

Amorphous PET Powder Preparation and Analysis. Micronized amorphous powder was produced from the above PET film by cryo-milling, first in an SM300 cutting mill (Retsch), then in a ZM200 centrifugal mill (Retsch), as described previously,[16] but using a ring sieve with a larger pore size (0.5 mm) in the second step. The powder was thoroughly dried at 45 °C for over 24 h before use as a substrate. PET crystallinity was determined before and after milling by DSC on a Netzsch DSC 214 Polyma. Measurements were performed in triplicate, with approximately 10 mg of samples in aluminum crucibles with lids. Samples were heated from 25

to 300 °C at 10 °C/min under a nitrogen atmosphere. Crystallinity was calculated using the equation: %Crystallinity $= \frac{\Delta H_m - \Delta H_c}{\Delta H_m^o}$, where ΔH_m is the enthalpy of melting of the sample, ΔH_c is the enthalpy of crystallization, and ΔH_m^o is the enthalpy of melting for a theoretical 100% crystallinity sample (140.1 J/g).

Cloning, Mutagenesis, and Library Creation. A codon-optimized gene from previous reports[16] encoding LCC-ICCG was obtained and subcloned into our pET21b(+)-GFP11 screening vector via *Nde*I and *Bam*HI sites. Briefly, pET21b-(+)-GFP11 was created by moving a stuffer containing the *Nde*I/*Bam*HI-linker-GFP11 fragment from ref 44 into pET21b(+) (Novagen, Millipore Sigma) via *Nde*I and *Xho*I sites. The DNA sequence showing LCC-ICCG inserted in pET21b(+)-GFP11 is indicated in Table S6. Plasmids were transformed into *E. coli* BL21 Gold (DE3) cells (B F⁻ *ompT hsdS*(rB⁻ mB⁻) *dcm*⁺ Tet^r gal λ(DE3) *endA* Hte; New England Biolabs). Chemical transformation was used for routine cloning, whereas in-house electrocompetent cells were used for library transformations. Cells were routinely cultured using either LB Miller agar or LB Miller liquid media, with relevant selection (carbenicillin, 100 μg mL⁻¹). Subcloning into the pET21b(+) expression vector was done by amplification of selected genes with the *Nde*I and *Xho*I sites, followed by digestion and ligation into pET21b(+) between the respective restriction sites to create a protein with a noncleavable C-terminal His₆ tag.

Libraries were created using a DNA shuffling protocol adapted from Waldo.[56] Briefly, template genes were amplified by Q5 DNA polymerase and then fragmented by DNaseI (Invitrogen). DNA fragments were then reassembled and amplified using Exo(−) Pfu DNA polymerase (Agilent). Full-length library gene fragments were cloned into pET21b(+)-GFP11 via *Nde*I and *Bam*HI sites following digestion with the appropriate restriction enzymes and ligation with T4 DNA Ligase at 16 °C overnight. The ligated library was transformed into electrocompetent *E. coli* BL21(DE3) Gold cells, which were selected on LB Miller plates with carbenicillin. Plates were streaked with all colonies into liquid media, and 1.0 OD₆₀₀ stocks were made prior to screening.

HT Coscreening Assay. *E. coli* libraries were first plated on Durapore PVDF 0.45 μm 47 mm membrane filters (product HVLP14250; Merck Millipore) on LB agar plates with carbenicillin. Cells were plated at approximately a 2.5 × 10⁵ dilution from a 1.0 OD₆₀₀ freezer cell stock to provide a well-spread density of cells on the plate. Plates were then grown overnight at 30 °C. Following this, membranes were transferred onto LB agar plates with carbenicillin and IPTG (1 mM) and incubated for 2 h at 37 °C. Membranes were then placed onto BHET screening plates. Small holes were poked through each membrane and plate to allow easy realignment of membranes to plates later. The first step to casting a BHET screening plate was to make a final 2.5% (w/v) agarose in 100 mM sodium phosphate pH 8 buffer solution. The BHET solution (at a working concentration of 500 mM BHET in 100% DMSO) was then added to the agarose solution (in 50 mL of total aliquots) to the appropriate concentration (ranging from 20 to 120 mM BHET), then mixed well, poured into a 50 mm Petri dish (Fisher Scientific), and then cooled.

For coarse screening, libraries of colonies were partially lysed by spraying with BugBuster (Millipore) 2−3 times from a spray bottle, rotating the plate to ensure even coverage, and

lysis of colonies. After each spray, the plates were allowed to dry. Once they were dry, membranes were removed and stored at 4 °C on LB agar plates. BHET screening plates were then wrapped to prevent evaporation and then incubated at relevant heat treatment and screening temperatures. For all high-temperature incubations, VWR hybridization ovens (VWR; model 5420) were used. The reaction time varied from 5 to 24 h. Following the reaction, concentrated solutions of refolded GFP1−10 in [100 mM Tris-HCl pH 7.4, 150 mM NaCl, and 10% (v/v) glycerol] (TNG buffer) were put on BHET screening plates. GFP1−10 was refolded from inclusion bodies as previously prescribed[44,57] then incubated on a nutator for 4 h to overnight. Longer incubation times with GFP1−10 can increase the fluorescent signal but also result in high background. Plates were then imaged using a ChemiDoc MP Imager (Bio-Rad) for detecting both colorimetric blot and Alexa 488 signals. Membranes containing partially lysed colonies were then realigned on BHET screening plates, and colonies were picked into 96-well plates containing LB medium based on the clearing zone appearance (indicator of enzyme activity) and fluorescent signals (indicator of the amount of enzyme presented) for subsequent fine screening.

For validation of colony lysis homogeneity on BHET screening plates, sfCherry[58] was used as a reference. A DNA fragment encoding for sfCherry was cloned into pET21b(+) via *Nde*I and *Xho*I. The plasmid was transformed into *E. coli* BL21 Gold (DE3) cells, diluted 1:5000 into enzyme libraries, and plated on Durapore membranes as described above. Following lysis on the membranes, the membranes were removed and BHET screening plates were imaged using a ChemiDoc MP Imager (Bio-Rad) with Alexa 546 blot analysis to check the homogeneity of red fluorescent intensity − an indicator of homogeneous colony lysis.

For fine screening, colonies with improved performance selected from libraries were grown in 96-well plates overnight at 37 °C and 250 rpm and then replica stamped (Boekel Scientific; model 140500) onto Durapore membranes. The screening process was repeated as above, except here, 8 μL of BugBuster was pipetted onto each colony blot for cell lysis. For each 96-well plate cell culture, BHET hydrolysis was evaluated on two BHET agar plates, one at the same concentration that was used for the HTP coscreening assay, and the other was at an increased BHET concentration (20−40 mM higher concentration than on the screening plates) and incubated for a longer reaction time (up to 48 h). BHET hydrolysis was monitored over time by taking images of the BHET agar plates with a Bio-Rad ChemiDoc MP under colorimetric blot every hour after incubation for the first 6 h and then for 15, 24, 36, and up to 48 h. Colonies chosen from this fine screening were labeled as putative improved variants.

Screening and Validation of Putative hits' Catalytic Performance on PET Substrate. Putative improved variants (and benchmarks) were expressed in small-scale, 1−5 mL of LB. Overnight cultures of colonies were seeded 1:100 volume into LB media with antibiotics in either 96 deep-well or 24-well plates (Fisher Scientific) and grown to 0.6−0.8 OD$_{600}$ at 37 °C and 250 rpm. Cultures were then induced with IPTG (1 mM) and grown for an additional 5 h at 37 °C, 250 rpm. Cultures were pelleted at 3500 rpm for 20 min, media was removed, and pellets were resuspended in 500 μL of lysis buffer [20 mM Tris-HCl pH 8 and 300 mM NaCl] and lysed by sonication with a Fisherbrand Model 50 Sonic Dismembrator (Fisher Scientific). Sonication was 5 × 20 s, on ice, centrifuging at 14

000 rpm for 3 min at 4 °C between cycles, with a final centrifuge for 30 min to clarify cell lysate.

Enzyme concentration was quantified by complementation of the cell lysates with GFP1−10 and measuring fluorescence intensity using a plate reader. Briefly, 20 μL of purified sulfide reductase-GFP11 construct (see ref 44 with a known concentration or 20 μL of cell lysates were added to Corning MaxiSorp 96-well plates, and 180 μL of refolded GFP1−10 in TNG buffer were added and incubated overnight at room temperature with gentle shaking. Proteins were quantified via a standard curve from 2-fold serial dilutions of a purified sulfide reductase-GFP11 construct (from 0.11 to 14.26 μM). The background fluorescence was subtracted from all samples using an equal volume of the cell lysate of an expression construct lacking the GFP11 tag [i.e., LCC in pET21b(+)] as a reference. Fluorescence was measured using a Tecan M Plex Plate Reader (excitation: 488 nm; emission: 520 nm). GFP1−10 complementation was performed in triplicate to verify the protein concentration.

All proteins were normalized to 1 μM using lysis buffer and diluted 1:10 (to 0.1 μM) in reactions containing 100 mM sodium phosphate buffer, pH 8, and 0.92% (w/v) amorphous PET coupons (Goodfellow Cambridge Ltd. product #ES301445; 9.4% crystallinity as 3 mm hole-punched circles (approximately 2.5 mg each; Fiskars) or 1% high-crystallinity PET powder (Goodfellow Cambridge Ltd. product #ES306031; 41.8% crystallinity[50]). Reactions were then incubated in deep-well 96-well plates at 68 °C, with aliquots drawn at each time point: 2, 4, 6, 8, 10, 12, and 24 h. To prevent evaporation over long reaction times, plates were sealed with aluminum plate foil (Thermo Scientific, product 232698) and wrapped in plastic. Edge wells of 96-well plates were not used to prevent the inconsistent evaporation of samples. At time points, new foils were used to reseal plates. No detectable evaporation occurred within 24 h reaction times. As necessary, results in 96-well plates could be verified with samples/reactions in single, airtight cryo-vials (Simport Scientific; product T309−2A). Absorbance at 240 nm was measured using a Tecan M Plex Plate Reader to detect aggregate aromatic products released,[33] with baseline (*t* = 0) absorbance for each enzyme subtracted from time points. BHET equivalent concentrations were determined from a standard curve of the absorbance of diluted BHET solutions. Promising enzyme variants were grown, and plasmids were isolated and sequenced. Plasmids from any promising variants were used as parents for additional rounds of evolution (via DNA shuffling).

Engineering LCC. A DNA fragment encoding LCC-WT was used as a starting template to create random mutation libraries, cloned into the pET21b(+)-GFP11 vector, and transformed into *E. coli* as described above. Enzyme libraries were then screened using the HT coscreening assay, with coarse screening first performed, followed by fine screening. In the first round, the library was coarse screened on 20 mM BHET agar plates at 65 °C after 5 h of reaction. Colonies that displayed higher BHET hydrolytic activity (larger clearing zones) and/or higher enzyme solubility (brighter green fluorescence) were picked and grown in a 96-well plate format as previously described. Putative hits were then selected after fine screening on BHET agar plates at 20 and 40 mM concentrations at 65 °C, up to 24 h of reaction time. Selected enzyme variants were then pooled together as parents for the second round of directed evolution, with the coarse screening

assay done at 40 mM BHET concentration, at 68 °C for 7 h, and the fine screening assay performed on 40 and 60 mM BHET agar plates at 68 °C and monitored for up to 24 h of reaction time. Validation assays were performed for enzyme variants selected from the second round along with starting template LCC-WT and benchmark LCC-ICCG.

A disulfide bond (D238C−S283C) was added to the best variant from the second round (LCC-F2) and LCC-P38L by single-point mutagenesis. The third round of evolution was done with coarse screening performed on 60 mM BHET agar plates at 70 °C for 20 h, with subsequent fine screening performed on 60 and 80 mM BHET agar plates at 70 °C for up to 48 h. To engineer new LCC variants with enhanced hydrolysis performance on amorphous PET coupons, the LCC-F6 variant selected from the third round was used as a template, and the fourth round of directed evolution was performed on 80 mM BHET agar plates at 70 °C for 20 h, with fine screening validated on both 80 and 100 mM BHET agar plates at 70 °C for up to 48 h.

The thermostability properties were screened in the final round of directed evolution by preheat treatment at 80 °C for 1 h of BHET agar plates in coarse screening, prior to the BHET hydrolysis reaction at 70 °C. BHET concentrations were also increased to 90 mM in coarse screening with a longer reaction time of 20 h. Fine screening was performed with both 90 and 120 mM BHET agar plates with up to 48 h of incubation at 70 °C. After the fifth round of directed evolution, the variant LCC-LANL was selected for final characterization.

Protein Expression and Purification. All proteins were expressed in the pET21b(+) vector using His$_6$ tag purification with Co TALON Resin (Takara Bio). Fresh colonies of each cell stock were picked, streaked out on LB selection plates, and grown overnight in LB media at 37 °C and 250 rpm. Cultures were then inoculated 1:1000 into 500 mL 2XYT media with carbenicillin, grown to 0.6−0.8 OD$_{600}$ at 37 °C, 250 rpm, and induced with 1 mM IPTG after being cooled for 10 min on ice or at 4 °C. Cultures were then grown for an additional 16−20 h at 20 °C and 150 rpm. Cells were then harvested for 20 min at 3500 rpm and stored at −80 °C until purification.

For purification, pellets were thawed and resuspended in 30 mL of cold column buffer [20 mM Tris-HCl pH 8, 300 mM NaCl, 10% (v/v) glycerol]. Pellets were then sonicated using a Branson Digital Sonifier 450 at 80% amplitude for 10 min on ice, maintaining the temperature below 20 °C. The lysate was clarified by centrifugation for 1 h at 4 °C and 40 000 × g. Lysate was filtered with a 0.45 μm syringe filter and loaded onto 2.5 mL of resin equilibrated with column buffer. The lysate was incubated with the resin and rocked at 4 °C overnight. Purification was performed manually. The lysate was discarded, and the resin was washed with 15 column volumes (CVs) of column buffer [20 mM Tris-HCl pH 8, 300 mM NaCl, 10% (v/v) glycerol], 10 CVs of column buffer with 5 mM imidazole, 5 CVs of column buffer with 10 mM imidazole, and finally eluted with 5 CVs of column buffer with 250 mM imidazole. The eluted protein was verified for correct size and purity by SDS-PAGE gel by running alongside Protein Kaleidoscope Protein Standards (Bio-Rad). As necessary, purified protein samples were diluted in Laemmli Buffer (1× concentration) and were either not boiled or boiled at 100 °C for 20 min before loading on the gel. The purity of purified proteins was >90% (evaluated with Image Lab, Bio-Rad). Enzymes were then buffer exchanged using an Amicon 10 kDa cutoff filter (Millipore Sigma) with [20 mM Tris-HCl pH 8

and 300 mM NaCl], using the manufacturer's protocol. Aliquots of the enzymes were stored at −80 °C until they were used. The protein concentration was quantified by the Pierce BCA Protein Assay (Fisher Scientific) using the manufacturer's protocol.

Protein Thermostability Assay. Enzymes in cell lysates were normalized to the same concentration of 1 μM and incubated for 1 h in a thermal cycler (MJ Research model PTC-200) at a range of temperatures, from 50 to 90 °C, in reaction buffer [100 mM sodium phosphate pH 8] in PCR tubes. Following heat treatment, samples were transferred to 1.5 mL microtubes and centrifuged at 14 000 × g for 3 min. The supernatant was used to quantify the amount of soluble enzyme remaining by diluting 1:10 in a solution of GFP1−10 in TNG buffer (see ref[44] and incubated for 4 h overnight, shaking, at room temperature, in the wells of Corning MaxiSorp 96-well plates (Corning, NY, USA). The background fluorescence was subtracted from all samples. Fluorescence was measured using a Tecan M Plex Plate Reader (ex: 488 nm; em: 520 nm). All of the samples were performed in triplicate. The remaining protein was compared to the initial concentrations.

Enzyme Differential Scanning Calorimetry. Enzyme denaturation thermograms were acquired by DSC on a MicroCal PEAQ-DSC Automated instrument (Malvern Panalytical). Immediately prior to analysis, the samples were purified by size exclusion chromatography on a HiLoad Superdex 75 pg column (Cytiva) pre-equilibrated with [50 mM NaH$_2$PO$_4$/Na$_2$HPO$_4$, 100 mM NaCl, pH 7.5]. For each enzyme, thermograms were recorded in low feedback mode with the temperature raised from 50 to 110 °C at six different ramp rates: 0.1, 0.2, 0.4, 0.8, 1.6, or 3.2 °C/min. Buffer subtraction and baseline correction were performed using the instrument's control and analysis software. Each enzyme's thermogram data sets were fit to a single-step, irreversible unfolding model (i.e., native-to-denatured) using the CalFitter v2.0 Web server[59] which provides E_{act}, the activation energy for unfolding, and T_{act}, the temperature at which one enzyme molecule per second denatures.

Small-Scale PET Hydrolysis Reactions. Reactions were performed with 0.7 mg of enzyme/g of PET and 2.9% (w/v) loading PET in 500 μL of evaporation-proof cryo-vials (Simport Scientific; product T309−2A). Reactions were composed of PET, enzymes (diluted with lysis buffer), and 100 mM sodium phosphate buffer, pH 8. Time points were taken at 2, 4, 6, 8, 10, 12, and 24 h, incubating at the reaction temperature. Samples were taken for the absorbance measurement and HPLC analysis. For HPLC analysis, samples were immediately diluted 50% (v/v) with cold methanol and then filtered using a 0.2 μm plate filter with MultiScreen HTS Filter Plates (Millipore Sigma; product MSGVN2250). Absorbance measurement was performed as above.[33] Samples were stored at −20 °C until analysis. As appropriate, samples for absorbance and HPLC analyses were diluted with ultrapure water. All reactions were performed in triplicate.

Monomer Quantification. Monomers of TPA, MHET, and BHET were quantified by HPLC using an Agilent Technologies Infinity II 1260, equipped with a G7115A diode array detector (DAD), detecting a signal at 240 nm. Samples were analyzed using a protocol adapted from ref[60]. 10 μL of sample maintained at 10 °C were injected onto a Phenomenex Luna C18(2) (100 Å, 150 mm × 4.6 mm, 5 μm) at 40 °C. The mobile phase consisted of (A) 20 mM phosphoric acid in ultrapure water and (B) 100% methanol.

The flow rate was a constant of 1.2 mL/min for a total time of 10 min per sample. An A/B gradient program was used as follows: 80:20% at t = 0 min; a gradient to 35:65% by t = 7.5 min; and held constant at 80:20% from t = 7.51 to 10 min. A calibration curve from 0.1 to 500 mg/L was used for each analyte to determine concentrations. All reactions were performed in triplicate.

Analysis of Enzyme Maximal Rates. Enzyme maximal rates were determined from TPA and the sum of aromatic product plots from HPLC quantification. Best-fit lines and parameters were determined using GraphPad Prism with nonlinear regression, fitting with least-squares regression. Each replicate was considered an individual point for fitting, and slopes were additionally compared for significant differences using an extra sum-of-squares F test ($p < 0.05$). All slopes (for each enzyme in a given experiment) with different slopes differed significantly, with $p < 0.0001$. Goodness of fit was determined from the R^2 values.

PET Hydrolysis in pH-Controlled Bioreactors. Enzymatic PET hydrolysis reactions on a 100 mL scale were carried out in duplicate using Applikon MiniBio bioreactor systems with 250 mL glass vessels (Getinge AB) equipped with one marine impeller. Amorphous PET film of 0.25 mm thickness (Goodfellow) was cut into approximately 10 × 10 mm squares, washed with 70% EtOH, and incubated at 40 °C until completely dry. These PET film squares were added to the reactor at 2.9% (w/v) solids loading (i.e., 2.9 g substrate in total) suspended in either 100 mM sodium phosphate buffer, pH 8, or 50 mM sodium phosphate buffer, pH 7.5, with 100 mM NaCl. The suspension was pre-equilibrated to 65 °C with stirring at 400 rpm. The reaction was initiated by the addition of enzyme to 0.7 mg/g of PET (i.e., 2.03 mg of enzyme in total). Depolymerization reactions proceeded for 48 h with continuous pH control through the intermittent addition of 6 M NaOH using a peristaltic pump control module (Applikon my-Control). For the 16.5% (w/v) solid loading experiments at 68 °C, the same process was used but with an increased enzyme loading of 1 mg/g of PET (i.e., 16.5 mg of enzyme in total) to match the conditions promoted by ref[47] and a lengthened run time of either 72 h on amorphous PET powder or 96 h on amorphous PET film. At the end of each reaction, any remaining substrate was recovered by filtration through a Whatman glass microfiber filter (Cytiva) using a Büchner funnel. The retained solid residue was washed with ultrapure water to remove any precipitated salts and dried at 40 °C overnight prior to obtaining the residual dry weight, from which the percentage mass loss was calculated.

Sequence Analysis. The sequence of LCC-ICCG was used to initiate an automatically converging jackhmmer[61] search against the Uniref100[62] database to identify homologous sequence clusters, with an E-value cutoff of 1E-50. The full sequences of the hits were aligned using ClustalOmega,[63] and compared to check if the mutations discovered in our directed evolution campaign were novel or found in existing natural homologues.

Structural Analysis. The X-ray crystallographic structure of LCC-ICCG in complex with 1,4-butanediol terephthalate (PDB: 8JMP) was used as a starting point for molecular modeling. Homology models of the active form (A165S), individual point mutations, and the final mutant incorporating the individual mutations were generated and analyzed using the FastDesign protocol in the Rosetta macromolecular modeling suite. A tetramer of ethylene terephthalate was computationally generated and used in flexible docking against the original LCC-ICCG structure and the homology model structure of the final mutant. Additional analyses were performed, pertaining to the occurrence of voids and unsatisfied hydrogen bonds in the enzyme structure and at the protein–substrate interface. For the interface, shape and charge complementarity, as well as molecular strains and clashes, were evaluated. All molecular renderings and visual analyses were performed in PyMOL 2.5.7 (Schrodinger). MOLE2.0 was used to evaluate voids, tunnels, and channels in protein structures. All scripts used in the modeling and analysis of the LCC enzyme structures will be provided upon request.

ASSOCIATED CONTENT

Data Availability Statement
All information can be made available from the corresponding author upon reasonable request. The nucleotide sequences of the following genes have been made available in GenBank with the corresponding accession numbers: LCC-WT (PQ223696), LCC-ICCG (PQ223702), LCC-F2 (PQ223697), LCC-F6 (PQ223698), LCC-B8 (PQ223699), LCC-C9 (PQ223700), and LCC-LANL (PQ223701).

Supporting Information
The Supporting Information is available free of charge at https://pubs.acs.org/doi/10.1021/acscatal.4c04321.

> Protein and DNA sequences of LCC variants and screening vector; analysis of reaction product ratios; sequence analysis of LCC variants; details for screening protocol; analysis of mutants along evolutionary trajectory; protein gel for final proteins tested; activity of enzymes at 65 and 70 °C with amorphous PET coupons over shorter and longer time scales; enzyme DSC and temperature survivability analysis; activity of enzymes on amorphous and high-crystallinity PET powder; polymer DSC analysis; details of structural analysis (PDF)

AUTHOR INFORMATION

Corresponding Author
Hau B. Nguyen − *Bioscience Division, Los Alamos National Laboratory, Los Alamos, New Mexico 87545, United States; BOTTLE Consortium, Golden, Colorado 80401, United States;* ● orcid.org/0000-0003-0174-9622; Phone: +1-505-667-5561; Email: hau@lanl.gov

Authors
Thomas M. Groseclose − *Bioscience Division, Los Alamos National Laboratory, Los Alamos, New Mexico 87545, United States; BOTTLE Consortium, Golden, Colorado 80401, United States;* ● orcid.org/0000-0001-7831-4294

Erin A. Kober − *Bioscience Division, Los Alamos National Laboratory, Los Alamos, New Mexico 87545, United States; BOTTLE Consortium, Golden, Colorado 80401, United States;* ● orcid.org/0009-0002-4354-1360

Matilda Clark − *BOTTLE Consortium, Golden, Colorado 80401, United States; Centre for Enzyme Innovation, School of the Environmental and Life Sciences, University of Portsmouth, Portsmouth PO1 2DT, U.K.*

Benjamin Moore − *BOTTLE Consortium, Golden, Colorado 80401, United States; Centre for Enzyme Innovation, School of the Environmental and Life Sciences, University of Portsmouth, Portsmouth PO1 2DT, U.K.*

Shounak Banerjee − *Bioscience Division, Los Alamos National Laboratory, Los Alamos, New Mexico 87545, United States; BOTTLE Consortium, Golden, Colorado 80401, United States;* ◉ orcid.org/0000-0001-6015-8908

Victoria Bemmer − *BOTTLE Consortium, Golden, Colorado 80401, United States; Centre for Enzyme Innovation, School of the Environmental and Life Sciences, University of Portsmouth, Portsmouth PO1 2DT, U.K.*

Gregg T. Beckham − *BOTTLE Consortium, Golden, Colorado 80401, United States; Renewable Resources and Enabling Sciences Center, National Renewable Energy Laboratory, Golden, Colorado 80401, United States;* ◉ orcid.org/0000-0002-3480-212X

Andrew R. Pickford − *BOTTLE Consortium, Golden, Colorado 80401, United States; Centre for Enzyme Innovation, School of the Environmental and Life Sciences, University of Portsmouth, Portsmouth PO1 2DT, U.K.;* ◉ orcid.org/0000-0002-7237-0030

Taraka T. Dale − *Bioscience Division, Los Alamos National Laboratory, Los Alamos, New Mexico 87545, United States; BOTTLE Consortium, Golden, Colorado 80401, United States*

Complete contact information is available at:
https://pubs.acs.org/10.1021/acscatal.4c04321

Author Contributions

Notes

■ ACKNOWLEDGMENTS

■ REFERENCES

(1) Carr, C. M.; Clarke, D. J.; Dobson, A. D. W. Microbial Polyethylene Terephthalate Hydrolases: Current and Future Perspectives. *Front. Microbiol.* **2020**, *11*, 571265.

(2) Carniel, A.; Waldow, V. D. A.; Castro, A. M. D. A comprehensive and critical review on key elements to implement enzymatic PET depolymerization for recycling purposes. *Biotechnol. Adv.* **2021**, *52*, 107811.

(3) Ellis, L. D.; Rorrer, N. A.; Sullivan, K. P.; Otto, M.; McGeehan, J. E.; Román-Leshkov, Y.; Wierckx, N.; Beckham, G. T. Chemical and biological catalysis for plastics recycling and upcycling. *Nat. Catal.* **2021**, *4* (7), 539−556.

(4) Tiso, T.; Narancic, T.; Wei, R.; Pollet, E.; Beagan, N.; Schröder, K.; Honak, A.; Jiang, M.; Kenny, S. T.; Wierckx, N.; Perrin, R.; Avérous, L.; Zimmermann, W.; O'Connor, K.; Blank, L. M. Towards bio-upcycling of polyethylene terephthalate. *Metab. Eng.* **2021**, *66*, 167−178.

(5) Wei, R.; von Haugwitz, G.; Pfaff, L.; Mican, J.; Badenhorst, C. P. S.; Liu, W.; Weber, G.; Austin, H. P.; Bednar, D.; Damborsky, J.; Bornscheuer, U. T. Mechanism-Based Design of Efficient PET Hydrolases. *ACS Catal.* **2022**, *12* (6), 3382−3396.

(6) Tournier, V.; Duquesne, S.; Guillamot, F.; Cramail, H.; Taton, D.; Marty, A.; André, I. Enzymes' Power for Plastics Degradation. *Chem. Rev.* **2023**, *123* (9), 5612−5701.

(7) Oda, K.; Wlodawer, A. Development of Enzyme-Based Approaches for Recycling PET on an Industrial Scale. *Biochemistry* **2024**, *63* (4), 369−401.

(8) Geyer, R.; Jambeck, J. R.; Law, K. L. Production, use, and fate of all plastics ever made. *Sci. Adv.* **2017**, *3* (7), No. e1700782.

(9) United Nations. *From Pollution to Solution: A global assessment of marine litter and plastic pollution*; United Nations Environment Programme, 2021.

(10) OECD. *Global Plastics Outlook Policy Scenarios To 2060*; Organization For Economic, 2022.

(11) Kawai, F.; Kawabata, T.; Oda, M. Current State and Perspectives Related to the Polyethylene Terephthalate Hydrolases Available for Biorecycling. *ACS Sustainable Chem. Eng.* **2020**, *8* (24), 8894−8908.

(12) Yoshida, S.; Hiraga, K.; Takehana, T.; Taniguchi, I.; Yamaji, H.; Maeda, Y.; Toyohara, K.; Miyamoto, K.; Kimura, Y.; Oda, K. A bacterium that degrades and assimilates poly(ethylene terephthalate). *Science* **2016**, *351* (6278), 1196−1199.

(13) Sulaiman, S.; Yamato, S.; Kanaya, E.; Kim, J.-J.; Koga, Y.; Takano, K.; Kanaya, S. Isolation of a novel cutinase homolog with polyethylene terephthalate-degrading activity from leaf-branch compost by using a metagenomic approach. *Appl. Environ. Microbiol.* **2012**, *78* (5), 1556−1562.

(14) Chen, S.; Tong, X.; Woodard, R. W.; Du, G.; Wu, J.; Chen, J. Identification and Characterization of Bacterial Cutinase*. *J. Biol. Chem.* **2008**, *283* (38), 25854−25862.

(15) Sonnendecker, C.; Oeser, J.; Richter, P. K.; Hille, P.; Zhao, Z.; Fischer, C.; Lippold, H.; Blázquez-Sánchez, P.; Engelberger, F.; Ramírez-Sarmiento, C. A.; et al. Low Carbon Footprint Recycling of Post-Consumer PET Plastic with a Metagenomic Polyester Hydrolase. *ChemSuschem* **2022**, *15*, No. e202101062.

(16) Erickson, E.; Gado, J. E.; Avilán, L.; Bratti, F.; Brizendine, R. K.; Cox, P. A.; Gill, R.; Graham, R.; Kim, D.-J.; König, G.; Michener, W. E.; Poudel, S.; Ramirez, K. J.; Shakespeare, T. J.; Zahn, M.; Boyd, E.

S.; Payne, C. M.; DuBois, J. L.; Pickford, A. R.; Beckham, G. T.; McGeehan, J. E. Sourcing thermotolerant poly(ethylene terephthalate) hydrolase scaffolds from natural diversity. *Nat. Commun.* **2022**, *13* (1), 7850.

(17) Tournier, V.; Topham, C. M.; Gilles, A.; David, B.; Folgoas, C.; Moya-Leclair, E.; Kamionka, E.; Desrousseaux, M. L.; Texier, H.; Gavalda, S.; Cot, M.; Guémard, E.; Dalibey, M.; Nomme, J.; Cioci, G.; Barbe, S.; Chateau, M.; André, I.; Duquesne, S.; Marty, A. An engineered PET depolymerase to break down and recycle plastic bottles. *Nature* **2020**, *580* (7802), 216−219.

(18) Son, H. F.; Cho, I. J.; Joo, S.; Seo, H.; Sagong, H.-Y.; Choi, S. Y.; Lee, S. Y.; Kim, K.-J. Rational Protein Engineering of Thermo-Stable PETase from Ideonella sakaiensis for Highly Efficient PET Degradation. *ACS Catal.* **2019**, *9* (4), 3519−3526.

(19) Pfaff, L.; Gao, J.; Li, Z.; Jäckering, A.; Weber, G.; Mican, J.; Chen, Y.; Dong, W.; Han, X.; Feiler, C. G.; Ao, Y.-F.; Badenhorst, C. P. S.; Bednar, D.; Palm, G. J.; Lammers, M.; Damborsky, J.; Strodel, B.; Liu, W.; Bornscheuer, U. T.; Wei, R. Multiple Substrate Binding Mode-Guided Engineering of a Thermophilic PET Hydrolase. *ACS Catal.* **2022**, *12* (15), 9790−9800.

(20) Lu, H.; Diaz, D. J.; Czarnecki, N. J.; Zhu, C.; Kim, W.; Shroff, R.; Acosta, D. J.; Alexander, B. R.; Cole, H. O.; Zhang, Y.; Lynd, N. A.; Ellington, A. D.; Alper, H. S. Machine learning-aided engineering of hydrolases for PET depolymerization. *Nature* **2022**, *604* (7907), 662−667.

(21) Bell, E. L.; Smithson, R.; Kilbride, S.; Foster, J.; Hardy, F. J.; Ramachandran, S.; Tedstone, A. A.; Haigh, S. J.; Garforth, A. A.; Day, P. J. R.; Levy, C.; Shaver, M. P.; Green, A. P. Directed evolution of an efficient and thermostable PET depolymerase. *Nat. Catal.* **2022**, *5* (8), 673−681.

(22) Then, J.; Wei, R.; Oeser, T.; Gerdts, A.; Schmidt, J.; Barth, M.; Zimmermann, W. A disulfide bridge in the calcium binding site of a polyester hydrolase increases its thermal stability and activity against polyethylene terephthalate. *FEBS Open Bio* **2016**, *6* (5), 425−432.

(23) Wei, R.; Oeser, T.; Schmidt, J.; Meier, R.; Barth, M.; Then, J.; Zimmermann, W. Engineered bacterial polyester hydrolases efficiently degrade polyethylene terephthalate due to relieved product inhibition. *Biotechnol. Bioeng.* **2016**, *113* (8), 1658−1665.

(24) Avilan, L.; Lichtenstein, B. R.; König, G.; Zahn, M.; Allen, M. D.; Oliveira, L.; Clark, M.; Bemmer, V.; Graham, R.; Austin, H. P.; Dominick, G.; Johnson, C. W.; Beckham, G. T.; McGeehan, J. E.; Pickford, A. R. Concentration-Dependent Inhibition of Mesophilic PETases on Poly(ethylene terephthalate) Can Be Eliminated by Enzyme Engineering. *ChemSuschem* **2023**, *16* (8), No. e202202277.

(25) Zhang, J.; Wang, H.; Luo, Z.; Yang, Z.; Zhang, Z.; Wang, P.; Li, M.; Zhang, Y.; Feng, Y.; Lu, D.; Zhu, Y. Computational design of highly efficient thermostable MHET hydrolases and dual enzyme system for PET recycling. *Commun. Biol.* **2023**, *6* (1), 1135.

(26) Akram, E.; Cao, Y.; Xing, H.; Ding, Y.; Luo, Y.; Wei, R.; Zhang, Y. On the temperature dependence of enzymatic degradation of poly(ethylene terephthalate). *Chin. J. Catal.* **2024**, *60*, 284−293.

(27) Wei, R.; Breite, D.; Song, C.; Gräsing, D.; Ploss, T.; Hille, P.; Schwerdtfeger, R.; Matysik, J.; Schulze, A.; Zimmermann, W. Biocatalytic Degradation Efficiency of Postconsumer Polyethylene Terephthalate Packaging Determined by Their Polymer Micro-structures. *Adv. Sci.* **2019**, *6* (14), 1900491.

(28) Tarazona, N. A.; Wei, R.; Brott, S.; Pfaff, L.; Bornscheuer, U. T.; Lendlein, A.; Machatschek, R. Rapid depolymerization of poly(ethylene terephthalate) thin films by a dual-enzyme system and its impact on material properties. *Chem. Catal.* **2022**, *2* (12), 3573−3589.

(29) Wei, R.; Oeser, T.; Barth, M.; Weigl, N.; Lübs, A.; Schulz-Siegmund, M.; Hacker, M. C.; Zimmermann, W. Turbidimetric analysis of the enzymatic hydrolysis of polyethylene terephthalate nanoparticles. *J. Mol. Catal. B: Enzym.* **2014**, *103*, 72−78.

(30) Then, J.; Wei, R.; Oeser, T.; Barth, M.; Belisário-Ferrari, M. R.; Schmidt, J.; Zimmermann, W. Ca2+ and Mg2+ binding site engineering increases the degradation of polyethylene terephthalate

films by polyester hydrolases from Thermobifida fusca. *Biotechnol. J.* **2015**, *10* (4), 592−598.

(31) Zumstein, M. T.; Kohler, H.-P. E.; McNeill, K.; Sander, M. High-Throughput Analysis of Enzymatic Hydrolysis of Biodegradable Polyesters by Monitoring Cohydrolysis of a Polyester-Embedded Fluorogenic Probe. *Environ. Sci. Technol.* **2017**, *51* (8), 4358−4367.

(32) Lusty Beech, J.; Clare, R.; Kincannon, W. M.; Erickson, E.; McGeehan, J. E.; Beckham, G. T.; DuBois, J. L. A flexible kinetic assay efficiently sorts prospective biocatalysts for PET plastic subunit hydrolysis. *RSC Adv.* **2022**, *12* (13), 8119−8130.

(33) Arnling Bååth, J.; Borch, K.; Westh, P. A suspension-based assay and comparative detection methods for characterization of polyethylene terephthalate hydrolases. *Anal. Biochem.* **2020**, *607*, 113873.

(34) Zhong-Johnson, E. Z. L.; Voigt, C. A.; Sinskey, A. J. An absorbance method for analysis of enzymatic degradation kinetics of poly(ethylene terephthalate) films. *Sci. Rep.* **2021**, *11* (1), 928.

(35) Wei, R.; Oeser, T.; Billig, S.; Zimmermann, W. A high-throughput assay for enzymatic polyester hydrolysis activity by fluorimetric detection. *Biotechnol. J.* **2012**, *7* (12), 1517−1521.

(36) Pfaff, L.; Breite, D.; Badenhorst, C. P. S.; Bornscheuer, U. T.; Wei, R. Chapter Twelve - Fluorimetric high-throughput screening method for polyester hydrolase activity using polyethylene terephthalate nanoparticles. *Methods Enzymol.* **2021**, *648*, 253−270.

(37) Shi, L.; Liu, P.; Tan, Z.; Zhao, W.; Gao, J.; Gu, Q.; Ma, H.; Liu, H.; Zhu, L. Complete Depolymerization of PET Wastes by an Evolved PET Hydrolase from Directed Evolution. *Angew. Chem., Int. Ed.* **2023**, *62* (14), No. e202218390.

(38) Molitor, R.; Bollinger, A.; Kubicki, S.; Loeschcke, A.; Jaeger, K.-E.; Thies, S. Agar plate-based screening methods for the identification of polyester hydrolysis by Pseudomonas species. *Microb. Biotechnol.* **2020**, *13* (1), 274−284.

(39) Branson, Y.; Badenhorst, C. P. S.; Pfaff, L.; Buchmann, C.; Wei, R.; Bornscheuer, U. T. High-Throughput Screening for Thermostable Polyester Hydrolases. In *Metagenomics: Methods in Molecular Biology*, Streit, W. R.; Daniel, R., Eds.; Humana, 2023, pp 153165. .

(40) Bayer, T.; Pfaff, L.; Branson, Y.; Becker, A.; Wu, S.; Bornscheuer, U. T.; Wei, R. Biosensor and chemo-enzymatic one-pot cascade applications to detect and transform PET-derived terephthalic acid in living cells. *iScience* **2022**, *25* (5), 104326.

(41) Dierkes Robert, F.; Wypych, A.; Pérez-García, P.; Danso, D.; Chow, J.; Streit, W. R. An Ultra-Sensitive Comamonas thiooxidans Biosensor for the Rapid Detection of Enzymatic Polyethylene Terephthalate (PET) Degradation. *Appl. Environ. Microbiol.* **2023**, *89* (1), No. e01603−01622.

(42) Pardo, I.; Jha, R. K.; Bermel, R. E.; Bratti, F.; Gaddis, M.; McIntyre, E.; Michener, W.; Neidle, E. L.; Dale, T.; Beckham, G. T.; Johnson, C. W. Gene amplification, laboratory evolution, and biosensor screening reveal MucK as a terephthalic acid transporter in Acinetobacter baylyi ADP1. *Metab. Eng.* **2020**, *62*, 260−274.

(43) Cribari, M. A.; Unger, M. J.; Unarta, I. C.; Ogorek, A. N.; Huang, X.; Martell, J. D. Ultrahigh-Throughput Directed Evolution of Polymer-Degrading Enzymes Using Yeast Display. *J. Am. Chem. Soc.* **2023**, *145* (50), 27380−27389.

(44) Cabantous, S.; Terwilliger, T. C.; Waldo, G. S. Protein tagging and detection with engineered self-assembling fragments of green fluorescent protein. *Nat. Biotechnol.* **2005**, *23* (1), 102−107.

(45) Santos-Aberturas, J.; Dörr, M.; Waldo, G. S.; Bornscheuer, U. T. In-Depth High-Throughput Screening of Protein Engineering Libraries by Split-GFP Direct Crude Cell Extract Data Normalization. *Chem. Biol.* **2015**, *22* (10), 1406−1414.

(46) Santos-Aberturas, J.; Dörr, M.; Bornscheuer, U. T. Normalized Screening of Protein Engineering Libraries by Split-GFP Crude Cell Extract Quantification. In *Protein Engineering: Methods in Molecular Biology*, Bornscheuer, U.; Höhne, M. Eds.; Humana Press, 2018, pp 157170. .

(47) Arnal, G.; Anglade, J.; Gavalda, S.; Tournier, V.; Chabot, N.; Bornscheuer, U. T.; Weber, G.; Marty, A. Assessment of Four

Engineered PET Degrading Enzymes Considering Large-Scale Industrial Applications. *ACS Catal.* **2023**, *13*, 13156−13166.

(48) Brizendine, R. K.; Erickson, E.; Haugen, S. J.; Ramirez, K. J.; Miscall, J.; Salvachúa, D.; Pickford, A. R.; Sobkowicz, M. J.; McGeehan, J. E.; Beckham, G. T. Particle Size Reduction of Poly(ethylene terephthalate) Increases the Rate of Enzymatic Depolymerization But Does Not Increase the Overall Conversion Extent. *ACS Sustainable Chem. Eng.* **2022**, *10* (28), 9131−9140.

(49) Singh, A.; Rorrer, N. A.; Nicholson, S. R.; Erickson, E.; DesVeaux, J. S.; Avelino, A. F. T.; Lamers, P.; Bhatt, A.; Zhang, Y.; Avery, G.; Tao, L.; Pickford, A. R.; Carpenter, A. C.; McGeehan, J. E.; Beckham, G. T. Techno-economic, life-cycle, and socioeconomic impact analysis of enzymatic recycling of poly(ethylene terephthalate). *Joule* **2021**, *5* (9), 2479−2503.

(50) Cuthbertson, A. A.; Lincoln, C.; Miscall, J.; Stanley, L. M.; Maurya, A. K.; Asundi, A. S.; Tassone, C. J.; Rorrer, N. A.; Beckham, G. T. Characterization of polymer properties and identification of additives in commercially available research plastics. *Green Chem.* **2024**, *26*, 7067−7090.

(51) Graham, R.; Erickson, E.; Brizendine, R. K.; Salvachúa, D.; Michener, W. E.; Li, Y.; Tan, Z.; Beckham, G. T.; McGeehan, J. E.; Pickford, A. R. The role of binding modules in enzymatic poly(ethylene terephthalate) hydrolysis at high-solids loadings. *Chem. Catal.* **2022**, *2* (10), 2644−2657.

(52) Uekert, T.; DesVeaux, J. S.; Singh, A.; Nicholson, S. R.; Lamers, P.; Ghosh, T.; McGeehan, J. E.; Carpenter, A. C.; Beckham, G. T. Life cycle assessment of enzymatic poly(ethylene terephthalate) recycling. *Green Chem.* **2022**, *24* (17), 6531−6543.

(53) Leman, J. K.; Weitzner, B. D.; Lewis, S. M.; Adolf-Bryfogle, J.; Alam, N.; Alford, R. F.; Aprahamian, M.; Baker, D.; Barlow, K. A.; Barth, P.; Basanta, B.; Bender, B. J.; Blacklock, K.; Bonet, J.; Boyken, S. E.; Bradley, P.; Bystroff, C.; Conway, P.; Cooper, S.; Correia, B. E.; Coventry, B.; Das, R.; De Jong, R. M.; DiMaio, F.; Dsilva, L.; Dunbrack, R.; Ford, A. S.; Frenz, B.; Fu, D. Y.; Geniesse, C.; Goldschmidt, L.; Gowthaman, R.; Gray, J. J.; Gront, D.; Guffy, S.; Horowitz, S.; Huang, P.-S.; Huber, T.; Jacobs, T. M.; Jeliazkov, J. R.; Johnson, D. K.; Kappel, K.; Karanicolas, J.; Khakzad, H.; Khar, K. R.; Khare, S. D.; Khatib, F.; Khramushin, A.; King, I. C.; Kleffner, R.; Koepnick, B.; Kortemme, T.; Kuenze, G.; Kuhlman, B.; Kuroda, D.; Labonte, J. W.; Lai, J. K.; Lapidoth, G.; Leaver-Fay, A.; Lindert, S.; Linsky, T.; London, N.; Lubin, J. H.; Lyskov, S.; Maguire, J.; Malmström, L.; Marcos, E.; Marcu, O.; Marze, N. A.; Meiler, J.; Moretti, R.; Mulligan, V. K.; Nerli, S.; Norn, C.; Ó'Conchúir, S.; Ollikainen, N.; Ovchinnikov, S.; Pacella, M. S.; Pan, X.; Park, H.; Pavlovicz, R. E.; Pethe, M.; Pierce, B. G.; Pilla, K. B.; Raveh, B.; Renfrew, P. D.; Burman, S. S. R.; Rubenstein, A.; Sauer, M. F.; Scheck, A.; Schief, W.; Schueler-Furman, O.; Sedan, Y.; Sevy, A. M.; Sgourakis, N. G.; Shi, L.; Siegel, J. B.; Silva, D.-A.; Smith, S.; Song, Y.; Stein, A.; Szegedy, M.; Teets, F. D.; Thyme, S. B.; Wang, R.Y.-R.; Watkins, A.; Zimmerman, L.; Bonneau, R. Macromolecular modeling and design in Rosetta: Recent methods and frameworks. *Nat. Methods* **2020**, *17* (7), 665−680.

(54) Li, A.; Sheng, Y.; Cui, H.; Wang, M.; Wu, L.; Song, Y.; Yang, R.; Li, X.; Huang, H. Discovery and mechanism-guided engineering of BHET hydrolases for improved PET recycling and upcycling. *Nat. Commun.* **2023**, *14* (1), 4169.

(55) Zeng, W.; Li, X.; Yang, Y.; Min, J.; Huang, J.-W.; Liu, W.; Niu, D.; Yang, X.; Han, X.; Zhang, L.; Dai, L.; Chen, C.-C.; Guo, R.-T. Substrate-Binding Mode of a Thermophilic PET Hydrolase and Engineering the Enzyme to Enhance the Hydrolytic Efficacy. *ACS Catal.* **2022**, *12* (5), 3033−3040.

(56) Waldo, G. S. Improving Protein Folding Efficiency by Directed Evolution Using the GFP Folding Reporter. In *Directed Enzyme Evolution. Methods in Molecular Biology*, Arnold, F. H.; Georgiou, G. Eds.; Humana Press, 2003, pp 343359. .

(57) Nguyen, H. B.; Terwilliger, T. C.; Waldo, G. S. Engineering an efficient and bright split Corynactis californica green fluorescent protein. *Sci. Rep.* **2021**, *11* (1), 18440.

(58) Nguyen, H. B.; Hung, L. W.; Yeates, T. O.; Terwilliger, T. C.; Waldo, G. S. Split green fluorescent protein as a modular binding partner for protein crystallization. *Acta Crystallogr., Sect. D: Biol. Crystallogr.* **2013**, *69* (12), 2513−2523.

(59) Kunka, A.; Lacko, D.; Stourac, J.; Damborsky, J.; Prokop, Z.; Mazurenko, S. CalFitter 2.0: Leveraging the power of singular value decomposition to analyse protein thermostability. *Nucleic Acids Res.* **2022**, *50* (W1), W145−w151.

(60) Knott, B. C.; Erickson, E.; Allen, M. D.; Gado, J. E.; Graham, R.; Kearns, F. L.; Pardo, I.; Topuzlu, E.; Anderson, J. J.; Austin, H. P.; Dominick, G.; Johnson, C. W.; Rorrer, N. A.; Szostkiewicz, C. J.; Copié, V.; Payne, C. M.; Woodcock, H. L.; Donohoe, B. S.; Beckham, G. T.; McGeehan, J. E. Characterization and engineering of a two-enzyme system for plastics depolymerization. *Proc. Natl. Acad. Sci. U. S. A.* **2020**, *117* (41), 25476−25485.

(61) Finn, R. D.; Clements, J.; Arndt, W.; Miller, B. L.; Wheeler, T. J.; Schreiber, F.; Bateman, A.; Eddy, S. R. HMMER web server: 2015 update. *Nucleic Acids Res.* **2015**, *43* (W1), W30−W38.

(62) Suzek, B. E.; Wang, Y.; Huang, H.; McGarvey, P. B.; Wu, C. H.; UniProt Consortium. UniRef clusters: A comprehensive and scalable alternative for improving sequence similarity searches. *Bioinformatics* **2015**, *31* (6), 926−932.

(63) Sievers, F.; Higgins, D. G. Clustal Omega for making accurate alignments of many protein sequences. *Protein Sci.* **2018**, *27* (1), 135−145.